博士学位論文

Preparation and Application of Functionalized Materials based on Poly(ε-caprolactone)
（ポリカプロラクトンを基盤とする機能性材料の創製と応用）

CAO　YU

2024 年 7 月

大阪大学大学院工学研究科

Contents

General Introduction

Polymer material

Materials have been one of the most significant factors shaping human civilization. Throughout history, humanity has utilized various materials, progressing from the Stone Age, to the Bronze Age, to the Iron Age, to the Glass Age, to the Steel Age, to the Aluminum Age, and currently to the Plastic (Polymer) Age.[1] As times have changed, so have people's demands on materials, resulting in shifts in the mainstream materials used in society, as noted in the historical progression.

Since the 20th century, the advent and development of polymer chemistry have led to the gradual integration of polymer materials into everyday life. Today, polymers hold a dominant position in material applications due to their unique and outstanding properties. These materials are not only low-cost and easy to manufacture, but they also offer excellent mechanical properties, low density, and remarkable durability. Polymer materials have become indispensable in contemporary society, finding widespread use in everything from simple packaging to heavy construction. Their versatility and efficiency have significantly contributed to the improvement and quality of life, underscoring their crucial role in meeting the daily needs of modern civilization.[2]

Advanced functional polymer

As people's demands for materials continue to evolve, it is becoming increasingly challenging for any single material to fully satisfy these needs, which has promoted the development of new polymers with specific functions. Such polymers are referred as advanced functional polymers, which hold significant potential for applications in various fields, including the wireless communication industry, biomimetic industries, oil-water separation, and intelligent industries. [3,4] Building on this potential, the interdisciplinary subject of functional polymer science emerged in the 1960s, encompassing materials science, biology, energy, and environment.[5] Beyond the mechanical properties of traditional polymer materials, advanced functional polymer materials can also exhibit photosensitivity, conductivity and catalytic

properties, making them a crucial cornerstone in modern industry.

Environmental pollution

However, the extensive use of polymer materials also imposes a significant burden on the environment due to their persistence and difficulty in degrading, resulting in some harmful problems such as plastic pollution and textile pollution. This environmental impact highlights the need for sustainable approaches in the development and utilization of polymer materials.

In Japan, the amount of plastic waste in household garbage has been rising over the past few years, reaching 4.1 million tons in 2019 (**Figure 1**). [6] More than three-quarters (77.2%) of this waste is reported as containers and packaging. In terms of per capita plastic packaging waste emissions, Japan ranks the largest emitter in Asia, and second in the world.

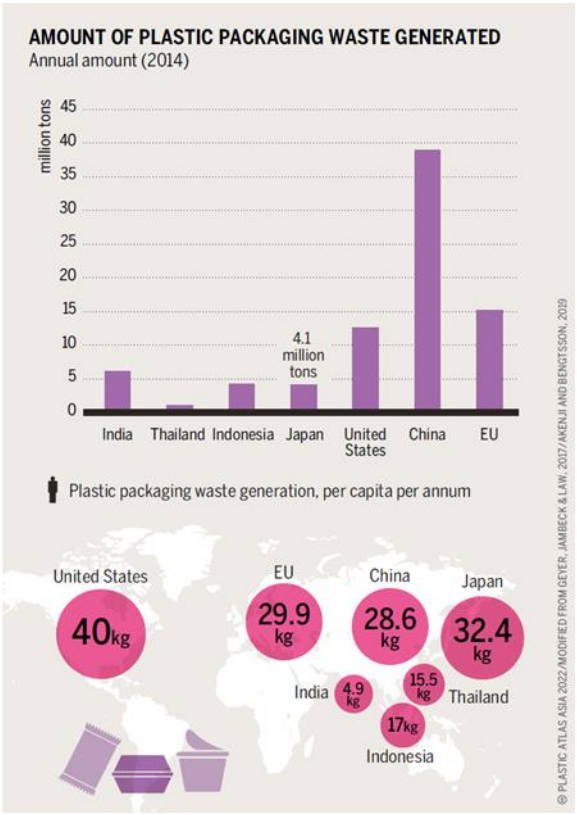

Figure 1. Amount of plastic packaging waste generated

On the other hand, only 22% of the materials are recycled properly. Most of polymers was disposed by incineration, resulting in an aggravation of air pollution and greenhouse effect. In response to this issue, the Japanese government established the Plastic Resource Circulation Strategy in 2019. This strategy emphasizes the importance of promoting alternatives to plastic and enhancing recycling efforts.

Biodegradable polymer

In response to the growing challenge of waste production and management, the European Union released its vision for a more sustainable plastics industry in 2018, to achieve this by

2030. In addition to promoting plastic recycling, the strategy addresses both the opportunities and risks associated with biodegradable polymers.[7]

Biodegradable polymers are polymeric materials that undergo degradation through the metabolic activity of naturally occurring organisms at least partially. [8] These polymers can function for a limited time before breaking down into non-toxic or environmentally benign residues under suitable conditions.[9] Based on the origin of their raw materials and manufacturing processes, biodegradable polymers are categorized into natural and synthetic types. Compared to natural polymers, synthetic biodegradable polymers offer distinct advantages, including the ability to be customized to achieve a broader range of properties and superior batch-to-batch uniformity. [9] Representative examples of synthetic biodegradable polymers include poly(lactic acid) (PLA), poly(lactide-co-glycolide), poly(vinyl alcohol), poly(caprolactone) (PCL), polyglycolic acid (PGA), poly(glycerol sebacate), and poly-β-hydroxybutyric acid. These polymers find extensive applications across various fields due to their biodegradable nature and tailored properties.

PCL

PCL was among the earliest polymers synthesized by the Carothers group in the early 1930s.[10] It is an aliphatic polyester known for its excellent biodegradability and biocompatibility, making it widely utilized in the biomedical field. PCL is a hydrophobic semi-crystalline polyester with a low glass transition temperature of -60 °C and a melting point ranging from 59 °C to 64 °C, facilitating easy formability at relatively low temperatures. [11] At body temperature, it exhibits a rubbery state with high permeability to low molecular substances. PCL demonstrates good thermal stability, with a thermal decomposition temperature in air exceeding 200 °C. As a semi-crystalline polymer, its crystallinity decreases with increasing molecular weight. Regardless of molecular weight, PCL follows a uniform crystallization process: nucleation occurs first, followed by gradual growth into spherulites, and ultimately forming large spherulites where the entire sample's crystalline phase connects. The crystallization behavior of PCL contributes significantly to its mechanical strength, enhancing its suitability for various applications.

PCL exhibits good solubility in various solvents at room temperature, such as chloroform, benzene, and cyclohexanone. It has low solubility in acetone, ethyl acetate, and dimethylformamide, and is insoluble in ethanol and ether. [12] Additionally, PCL boasts favorable mechanical properties and has received approval from the American Food and Drug Administration for biomedical applications.[13] Compared to conventional polymers such as polyethylene and polypropylene, which require hundreds or even thousands of years to fully degrade, PCL undergoes complete degradation in just 2-4 years, depending on its molecular weight. This rapid biodegradability, coupled with its thermoplasticity, has led to its widespread use across various applications.[14]

The degradation of polymers is influenced by various factors, including molecular weight, crystallinity, and morphology. [15] In the case of PCL, degradation primarily occurs in the amorphous region, leading to an increase in crystallinity as degradation progresses. This degradation process can be characterized as a two-stage process. Initially, hydrolytic cleavage of the ester bond takes place under physiological conditions, typically around 40°C. [16] Subsequently, the crystalline portion undergoes degradation facilitated by living organisms such as bacteria and fungi [17,18] present in various biological environments including lake water, soil, and river ecosystems. [19,20] The complete degradation pathway of PCL can be depicted in **Figure 2**.[16]

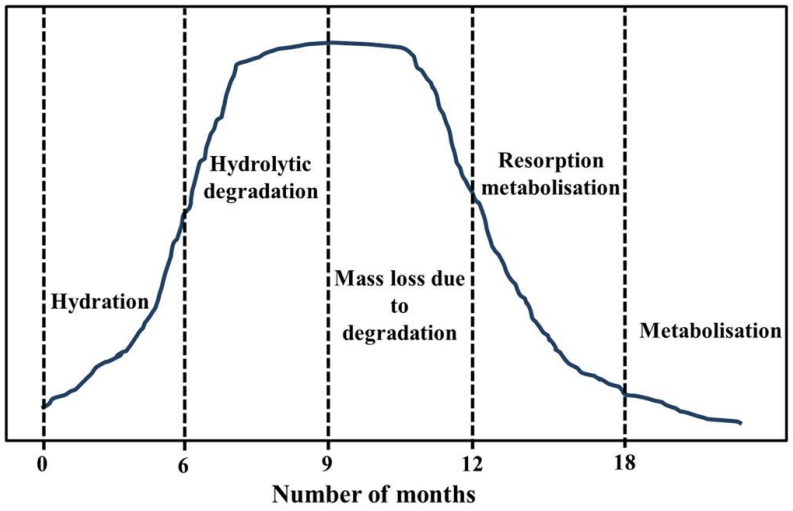

Figure 2. Graphical illustration of the complete degradation of PCL with respect to time.

When compared to commonly used biodegradable polymers like PLA and PGA, PCL exhibits a slower degradation rate (see **Table 1**). This characteristic led the medical device and drug delivery communities to perceive that faster resorbable polymers had fewer disadvantages,

due to PCL's longer degradation period (up to 3-4 years) and intracellular resorption pathways. Consequently, PCL was largely overlooked for nearly two decades. It wasn't until the 1990s that researchers recognized the potential of PCL's excellent rheological and viscoelastic properties. These attributes enabled the preparation of PCL into scaffolds, which were then applied in the field of tissue engineering. This resurgence of interest brought PCL back into the spotlight, demonstrating its capabilities and expanding its applications in biomedical research and development.

Table 1. Degradation time of different biodegradable polymers in vitro

Polymer	Melting point (°C)	Glass transition (°C)	Degradation time (months)
PLA[21,22]	173-178	60-65	6-24
PGA[23,24]	225-230	35-40	4-8
PCL[25,26]	55-64	-60	36-48

Functionalization of PCL

The widespread commercialization of PCL remains limited due to its inherent hydrophobicity and the absence of functional groups. Therefore, enhancing the functionalization of PCL is crucial. Moreover, the modification options for PCL are constrained by the limited availability of functional groups, necessitating suitable methods to broaden its applications. According to literature reports, six commonly used methods exist for modifying PCL, as depicted in **Figure 3**.

In general, the functionalization of PCL is achieved through blending with other polymers like PLA[27,28] or starch[29,30], or creating composite materials with additives such as hydroxyapatite[13,31] and calcium carbonate.[32,33] Copolymerization enables the direct production of complex and functional macromolecules, but it can be time-consuming and costly. In contrast, filler modification and surface modification methods offer the advantages of simplicity, making them more suitable for laboratory research. Functionalized PCL can be processed into films or monoliths tailored for various applications.

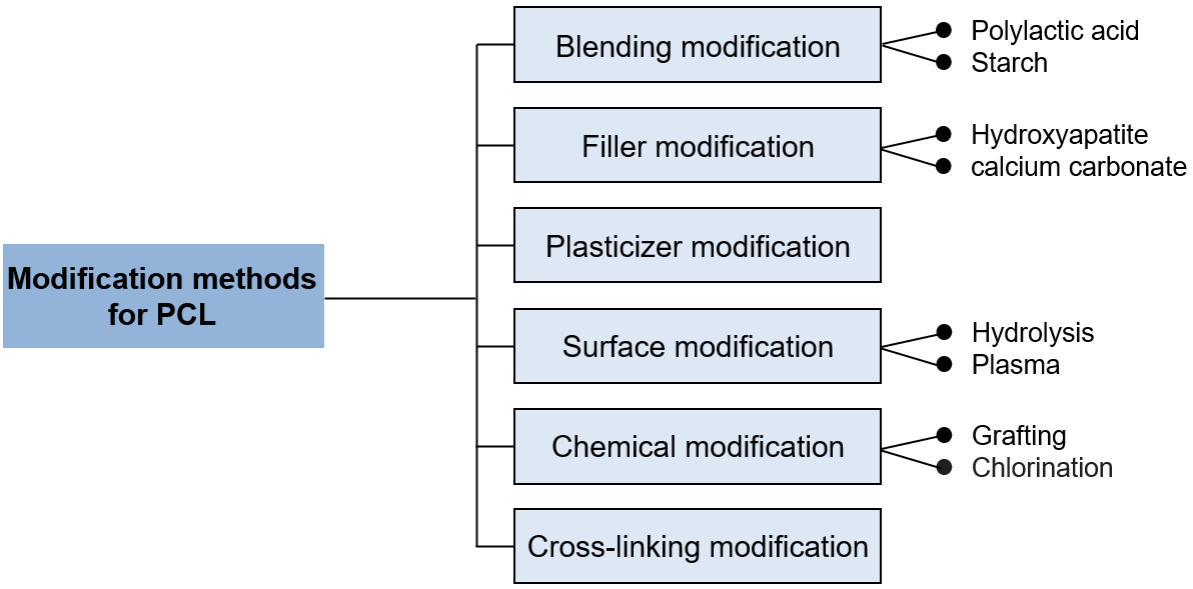

Figure 3. Commonly used modification methods for PCL.

PCL film

PCL film is a versatile biodegradable material that has garnered significant attention for its unique properties and diverse applications. A key advantage of PCL film is its biodegradability, unlike traditional plastics, PCL can be broken down by microorganisms into non-toxic byproducts, thereby reducing environmental impact and promoting sustainability. Moreover, PCL film exhibits excellent processability and can be easily shaped using methods such as extrusion[34,35], molding[36,37] and solvent casting[38]. Its compatibility with other polymers allows for the creation of composite materials with tailored properties. PCL film finds applications across multiple fields. In biomedicine, it is utilized in drug delivery systems[39] and wound dressings[40,41] for its biocompatibility and controllable degradation rate. In packaging, PCL film serves as an eco-friendly alternative to disposable items, thereby mitigating plastic waste. Additionally, its use as biodegradable mulch in agriculture enhances soil quality and crop yields while minimizing environmental harm.[42,43]

In summary, the biodegradable nature, flexibility, and compatibility of PCL film position it as a valuable solution for addressing environmental challenges and driving innovation across various industries.

PCL monolith

The concept of "monolith" was introduced in the early 1990s, originally describing a novel chromatographic column technology designed for rapid biomolecule separation. [44,45] these columns are characterized by large through-holes that allow for high flow rates at low back pressure. Over decades of development, the types of monoliths have expanded, and their definition has broadened to encompass porous integral materials with continuous three-dimensional structures. Key features of monoliths include rich interconnected pore structures and large specific surface areas.

Monoliths exhibit a wide range of material selectivity, accommodating matrices made from metals[46,47], polymers[48,49], and inorganic materials[50,51]. The preparation methods for monoliths include bio-template techniques, gas foaming, 3D printing, and phase separation. Among these, the phase separation method is particularly suitable for laboratory research due to its simplicity and minimal equipment requirements.

Recently, PCL has gained attention for its excellent biocompatibility and biodegradability. PCL monoliths prepared via the phase separation method have shown significant potential in applications such as tissue engineering scaffolds[52,53] and oil/water separation applications[54]. These attributes have sparked considerable interest among researchers, highlighting the versatility and promising future of PCL monoliths in various fields.

Outline of this dissertation

In this dissertation, extensive research was undertaken to explore the functionalization of PCL using surface modification and filler modification methods. These methods involved introducing diverse functional groups onto the surfaces or throughout PCL-based materials. The goal was to enhance hydrophilicity, crucial for applications requiring improved interaction with aqueous environments, while simultaneously improving mechanical properties, such as tensile strength.

A pivotal achievement of this research was ensuring that the functionalization processes, whether at the surface or within the matrix, preserved the intrinsic chemical structure of PCL. This preservation is critical as it maintains PCL's original biodegradability, a fundamental

feature that enhances its appeal for sustainable and environmentally friendly applications. The biodegradability of PCL is particularly valuable in medical, environmental, and packaging fields, where materials capable of naturally degrading without environmental harm are highly sought after.

This dissertation aims to significantly advance the development of next-generation functionalized PCL materials by providing a detailed exploration of modification techniques and their impacts. It examines potential applications across various sectors, demonstrating how these advancements can address specific industrial and medical requirements. Through a blend of experimental studies and theoretical analyses, this research establishes a robust framework for future innovations in PCL functionalization, facilitating the creation of materials that are not only high-performing but also sustainable and environmentally responsible.

Chapter 1

In Chapter 1, PCL was functionalized by surface oxidation method using chlorine dioxide radical ($ClO_2^{\bullet}$) gas, facilitated by ultraviolet (UV) light irradiation (**Figure 4**). The study investigated the effects of oxidation duration and UV light intensity on elemental ratios, chemical components, and morphology. Additionally, a dye test was conducted to confirm the presence of carboxyl groups and to elucidate the underlying mechanism. Notably, UV light is solely required to activate $ClO_2^{\bullet}$ gas and is not essential for the modification process of the plastic surface.[55] In addition, electroless metal plating was

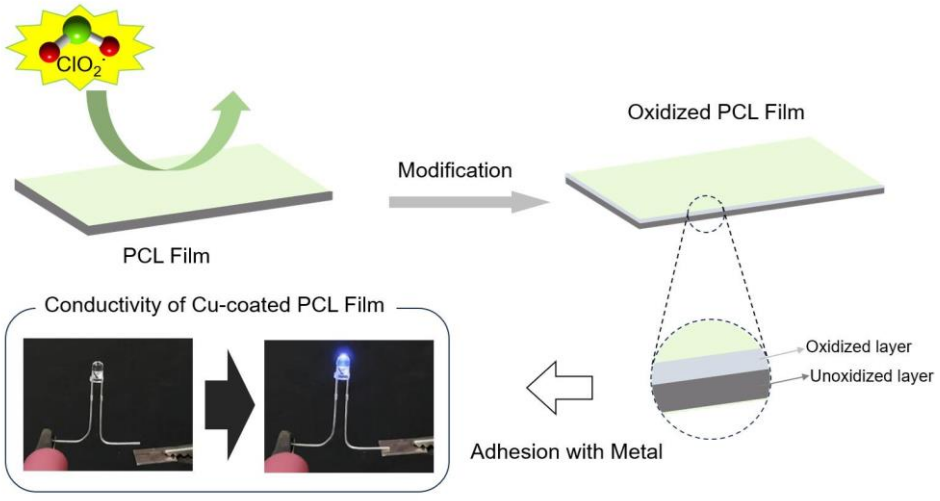

Figure 4. Graphical illustration of the surface modification of PCL film using chlorine dioxide radical gas and its composite with copper.

employed on oxidized PCL film to explore its potential applications. This approach is expected to expand the range of available materials suitable for polymer substrates coated with metal layers.

Chapter 2

In Chapter 2, a porous monolithic material was fabricated with a PCL matrix using the non-solvent thermally-induced phase separation (N-TIPS) method. Subsequently, surface modification of the PCL monolith was achieved using polydopamine (PDA) due to its strong adhesion property. The PDA-coated PCL monolith (PDA-PCL monolith) served as a catalyst support for dye wastewater treatment. In this study, gold (Au) particles were immobilized onto the surface of the PDA-PCL monolith, leveraging PDA's adhesion properties akin to double-sided tape. Furthermore, the catechol groups within PDA acted as reducing agents to convert Au^{3+} ions to Au, facilitating the formation of Au particles.[56] The resulting Au@PDA-PCL monolith was employed as a flow reactor using a peristaltic pump to degrade azo dyes in water. (**Figure 5**)

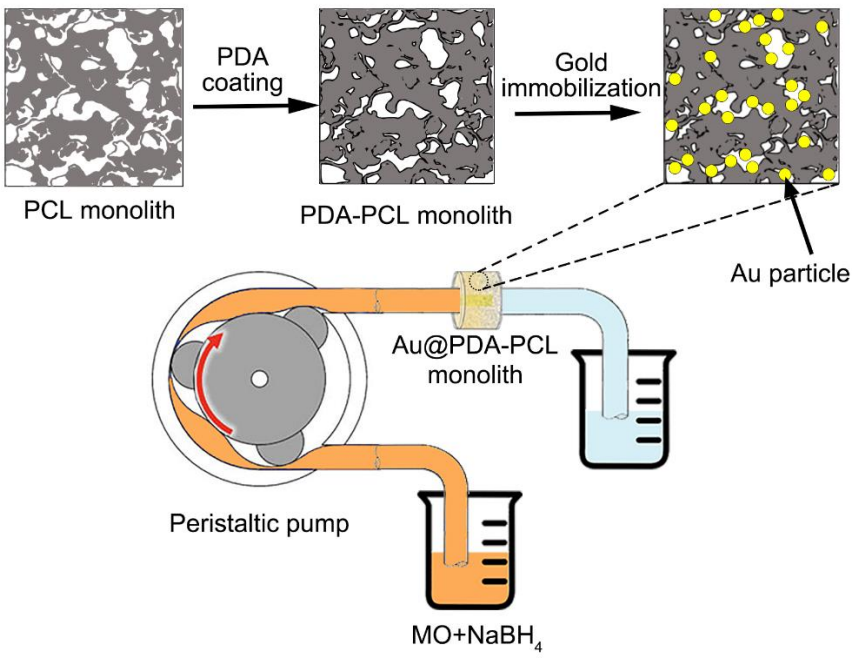

Figure 5. Graphical illustration of the surface modification of PCL monolith using polydopamine and its application in methyl orange degradation.

Chapter 3

In Chapter 3, a photoluminescent film incorporating PCL and nitrogen-doped carbon quantum dots (N-CQDs) with the function of information protection and encryption was prepared (**Figure 6**). The N-CQDs were synthesized from citric acid with urea as a dopant for the enhancement of fluorescent properties. The effect of dopant in chemical structure and luminescent properties of N-CQDs were investigated with different amounts of dopant. Then, the synthesized N-CQDs was utilized as a filler for the modification of PCL film, providing an enhanced hydrophilicity and mechanical properties. The appropriate crystallization temperature and degree of crystallinity of PCL provide the composite film with opaque characteristics at room temperature, rendering it an ideal carrier for carrying information. Importantly, the good photoluminescent properties of N-CQDs was preserved in PCL/N-CQDs composite film. Based on this, the information encryption and decryption were achieved using UV light.

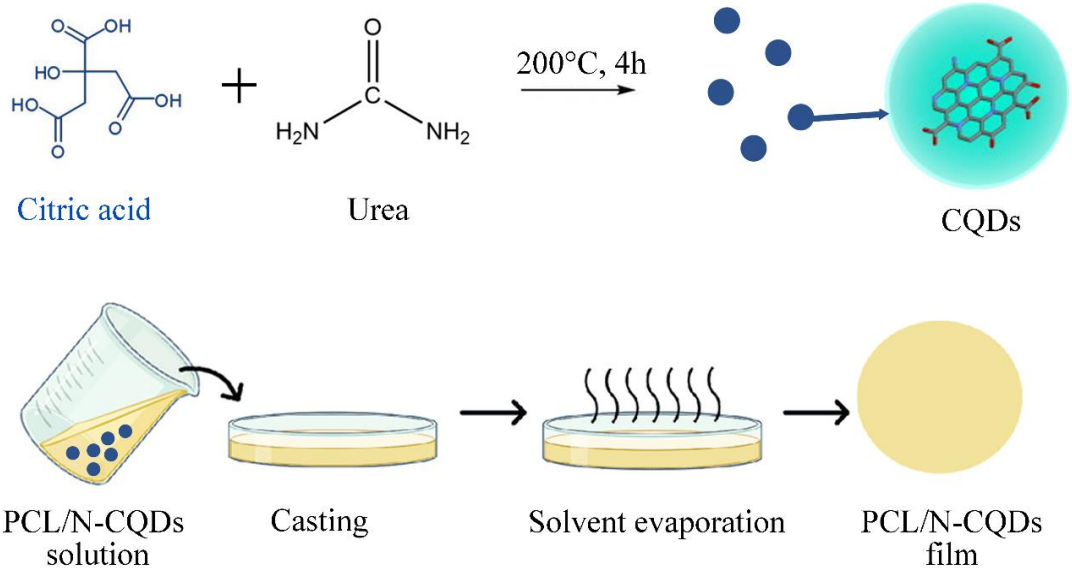

Figure 6. Graphical illustration of the filler modification of PCL with N-CQDs.

References

[1] I. O. Oladele, T. F. Omotosho, A. A. Adediran, *Int. J. Polym. Sci.*, **2020**, *2020*, 1.

[2] E. Rudnik, *CPM*, Second edition., Elsevier, Amsterdam, **2019**.

[3] F. Zhao, Y. Shi, L. Pan, G. Yu, *Acc. Chem. Res.*, **2017**, *50*, 1734.

[4] W. Zhang, B. Aguila, S. Ma, *J. Mater. Chem. A*, **2017**, *5*, 8795.

[5] B. C. Anderson, G. D. Andrews, P. Arthur, H. W. Jacobson, L. R. Melby, A. J. Playtis, W. H. Sharkey, *Macromolecules*, **1981**, *14*, 1599.

[6] P. J. Dickella Gamaralalage, A. Abeynayaka, M. Hayashi, *Jpn. Plast. Waste Manag. – Challenges Potential Solut.*, Heinrich Boell Stiftung Hong Kong Office, **2022**.

[7] T. P. Haider, C. Völker, J. Kramm, K. Landfester, F. R. Wurm, *Angew. Chem. Int. Ed.*, **2019**, *58*, 50.

[8] L. S. Nair, C. T. Laurencin, *Prog. Polym. Sci.*, **2007**, *32*, 762.

[9] X. Peng, K. Dong, Z. Wu, J. Wang, Z. L. Wang, *J. Mater. Sci.*, **2021**, *56*, 16765.

[10] F. J. V. Natta, J. W. Hill, W. H. Carothers, *J. Am. Chem. Soc.*, **1934**, *56*, 455.

[11] C. K. S. Pillai, C. P. Sharma, *J, Biomater, Appl.*, **2010**, *25*, 291.

[12] O. Coulembier, P. Degée, J. L. Hedrick, P. Dubois, *Progr, Polym, Sci.*, **2006**, *31*, 723.

[13] E. S. Permyakova, P. V. Kiryukhantsev-Korneev, K. Yu. Gudz, A. S. Konopatsky, J. Polčak, I. Y. Zhitnyak, N. A. Gloushankova, D. V. Shtansky, A. M. Manakhov, *Nanomaterials*, **2019**, *9*, 1769.

[14] M. A. Woodruff, D. W. Hutmacher, *Prog. Polym. Sci.*, **2010**, *35*, 1217.

[15] T. K. Dash, V. B. Konkimalla, *J. Control. Release.*, **2012**, *158*, 15.

[16] P. Mandal, R. Shunmugam, *J. Macromol. Sci. A*, **2021**, *58*, 111.

[17] H. Nishida, Y. Tokiwa, *J. Environ. Polym. Degr.*, **1993**, *1*, 227.

[18] C. V. Benedict, W. J. Cook, P. Jarrett, J. A. Cameron, S. J. Huang, J. P. Bell, *J, Appl. Polym. Sci.*, **1983**, *28*, 327.

[19] H. Yavuz, C. Babaç, *J. Polym. Environ.*, **2003**, *11*, 107.

[20] D. R. Chen, J. Z. Bei, S. G. Wang, *Polym. Degrad. Stab.*, **2000**, *67*, 455.

[21] C. Migliaresi, L. Fambri, D. Cohn, *J. Biomater. Sci. Polym. Ed.*, **1994**, *5*, 591.

[22] E. A. R. Duek, C. A. C. Zavaglia, W. D. Belangero, *Polymer*, **1999**, *40*, 6465.

[23] R. M. Ginde, R. K. Gupta, *J. Appl. Polym. Sci.*, **1987**, *33*, 2411.

[24] C. C. Chu, *J. Biomed. Mater. Res.*, **1981**, *15*, 795.

[25] B. Wang, Y. Li, G. Weng, Z. Jiang, P. Chen, Z. Wang, Q. Gu, *Compos. Sci. Technol.*, **2014**, *96*, 63.

[26] A. Gurarslan, Y. Caydamli, J. Shen, S. Tse, M. Yetukuri, A. E. Tonelli, *Biomacromolecules*, **2015**, *16*, 890.

[27] N. Mulchandani, K. Masutani, S. Kumar, H. Yamane, S. Sakurai, Y. Kimura, V. Katiyar, *Polym. Chem.*, **2021**, *12*, 3806.

[28] K. Sommer, D. Van Opdenbosch, C. Zollfrank, *Polymers*, **2023**, *15*, 455.

[29] J. H. Mina Hernandez, *Polymers*, **2020**, *13*, 38.

[30] A. Tampau, C. González-Martínez, A. Chiralt, *Polym. Degrad. Stab.*, **2020**, *173*, 109100.

[31] M. C. Azevedo, R. L. Reis, M. B. Claase, D. W. Grijpma, J. Feijen, *J. Mater. Sci. Mater. Med.*, **2023**, *14*, 103.

[32] J. Liang, L. Zhou, C. Tang, C. Tsui, *J. Appl. Polym. Sci.*, **2013**, *128*, 2940.

[33] J.-Y. Park, K.-H. Kyung, K. Tsukada, S.-H. Kim, S. Shiratori, *Polymer*, **2017**, *123*, 194.

[34] J. S. Lyu, J.-S. Lee, J. Han, *Sci, Rep.*, **2019**, *9*, 20236.

[35] T. J. Gutiérrez, J. R. Mendieta, R. Ortega-Toro, *Food Hydrocolloids*, **2021**, *111*, 106255.

[36] R. Ortega-Toro, I. Morey, P. Talens, A. Chiralt, *Carbohydrate Polymers*, **2015**, *127*, 282.

[37] I. Ferrer, A. Manresa, J. A. Méndez, M. Delgado-Aguilar, M. L. Garcia-Romeu, *Polymers*, **2021**, *13*, 2412.

[38] H. Lo, H. Kuo, Y. Huang, *Artificial Organs*, **2010**, *34*, 648.

[39] E. Schlesinger, N. Ciaccio, T. A. Desai, *Mater. Sci. Eng. C*, **2015**, *57*, 232.

[40] K. W. Ng, H. N. Achuth, S. Moochhala, T. C. Lim, D. W. Hutmacher, *J. Biomater. Sci. Polym. Ed.*, **2007**, *18*, 925.

[41] R. Augustine, N. Kalarikkal, S. Thomas, *Appl. Nanosci.*, **2016**, *6*, 337.

[42] N. A. F. Othman, S. Selambakkannu, N. Seko, *Energy. Nexus.*, **2022**, *8*, 100137.

[43] N. Yang, L. Ying, K. Li, F. Chen, F. Zhao, Z. Sun, L. Feng, J. Liu, *Polymers*, **2022**, *14*, 5340.

[44] Frantisek. Svec, J. M. J. Frechet, *Anal. Chem.*, **1992**, *64*, 820.

[45] F. Svec, J. M. J. Fréchet, *Science*, **1996**, *273*, 205.

[46] F. Liu, D. Feng, H. Yang, X. Guo, *Sci. Rep.*, **2020**, *10*, 4331.

[47] L. Zhang, T. Li, M. Zhang, Y. Li, *J. Rare Earths*, **2011**, *29*, 758.

[48] Y. Li, H. D. Tolley, M. L. Lee, *J. Chromatogr. A*, **2010**, *1217*, 8181.

[49] S. Yoneda, W. Han, U. Hasegawa, H. Uyama, *Polymer*, **2014**, *55*, 3212.

[50] B. Liu, L. Wu, X. Zhou, H. Wu, B. Zheng, *J. Mater. Chem. B*, **2018**, *6*, 824.

[51] L. Wang, F. Ai, Y. Liu, Y. Liu, *Mater. Lett.*, **2018**, *213*, 44.

[52] R. Scaffaro, F. Lopresti, L. Botta, S. Rigogliuso, G. Ghersi, *J. Mech. Behav. Biomed. Mater.*, **2016**, *63*, 303.

[53] N. Bahremandi Tolou, H. Salimijazi, T. Dikonimos, G. Faggio, G. Messina, A. Tamburrano, A. Aurora, N. Lisi, *J. Mater. Sci.*, **2021**, *56*, 5581.

[54] X. Yang, Z. Yin, X. Zhang, Y. Zhu, S. Zhang, *Polymer*, **2020**, *204*, 122852.

[55] Y. Jia, J. Chen, H. Asahara, T.-A. Asoh, H. Uyama, *ACS Appl. Polym. Mater.*, **2019**, *1*, 3452.

[56] J. Luo, N. Zhang, R. Liu, X. Liu, *RSC Adv.*, **2014**, *4*, 64816.

Chapter 1

Surface Oxidation of Poly(ε-caprolactone) Using Chlorine Dioxide Radical Gas

1-1. Introduction

In recent years, multi-functional polymers have gained widespread usage in various fields and have gradually replaced traditional materials such as metal and glass. This can be attributed to their superior properties, including chemical resistance and enhanced mechanical strength. Furthermore, they have the advantages of low cost, ease of fabrication, and lightweight. A metal coating on the surface of a polymer can significantly reduce the weight of the material while meeting the performance requirements of metallic materials. Consequently, polymer substrates coated with metal layers are required to achieve desired properties. To date, several methods have been reported in this field, such as fused deposition modeling[1-4] and selective laser sintering[5-7] using polyamide, PLA, and poly(ethylene terephthalate). The electroless plating method involves a catalytic redox reaction between metal ions in an aqueous solution and a chemical reagent.[8,9] This process, known for its cost-effectiveness and low-temperature demand, hosts the intriguing potential of coating polymer substrates with a wide range of metals only if the polymer surface is properly prepared to provide an appropriate catalyst for facilitating the electroless plating procedure.[10,11]

In the pursuit of eco-friendly development and plastic pollution waste mitigation, biodegradable polymers have gained significant attention in recent years. Moreover, biodegradable polymers, such as PLA, polybutylene succinate, poly(vinyl alcohol), and PCL, are promising lightweight materials. PCL is a synthetic biodegradable polymer that can be degraded into caprolactone in the natural environment and subsequently metabolized into CO_2 and H_2O in a short time owing to its ester group on the main chain.[12] However, the hydrophobicity of PCL restricts its wider applications, such as wastewater treatment and tissue engineering. Additionally, the modification options for PCL are limited owing to the scarcity of functional groups. Generally, PCL is modified either by copolymerization with other polymers, such as polyethylene glycol[13,14] or PLA[15,16], or by the fabrication of composite

materials, such as polydopamine[17,18] and calcium carbonate. Unfortunately, only a limited number of techniques have been reported for the direct modification of PCL-based materials.

Currently, diverse techniques are applied for the surface modification of materials, which can also be applied to the surface of PCL-based materials, such as plasma treatment,[19–21] laser treatment,[22–24] grafting,[25–27] and alkali treatment.[28–30] Nevertheless, these treatments suffer from high costs and hazardous operation conditions, making them less feasible, especially for materials with complex geometric shapes. Furthermore, another drawback arises from the stability of the polar functional groups introduced onto the surface, as observed with methods such as plasma treatment.[31,32] Previously, the effect of a light-activated chlorine dioxide radical ($ClO_2^{\bullet}$) as a potent oxidant was demonstrated in the conversion of methane to methanol and formic acid in a perfluorohexane environment under photoirradiation and ambient conditions (298 K, 1 atm).[33] In this process, the oxidant $ClO_2^{\bullet}$ was generated by acidification of a sodium chlorite ($NaClO_2$) solution (Equation 1-1). The chlorine radical ($Cl^{\bullet}$) generated from $ClO_2^{\bullet}$ was illuminated with UV light (Equation 1-2). In recent years, light-activated $ClO_2^{\bullet}$ has been extended to the surface oxidation of polymer substances such as polycarbonate,[34] polypropylene,[35] and poly(3-hydroxybutyrate-co-3-hydroxyhexanoate).[36] During this oxidation, the methyl groups in the polymer are oxidized to hydroxyl and carboxyl groups through interactions with the radical gas. Importantly, this oxidation process preserves the chemical integrity of the polymer matrix, yielding oxygen-enriched oxidized polymers suitable for future applications. Notably, research on polymers lacking methyl groups remains relatively scarce. Exploring the applicability of this oxidation method to other polymers devoid of side-chain methyl groups holds significant promise. Expanding our understanding in this area could unveil new avenues for surface modification techniques.

$$5NaClO_2+4HCl \rightarrow 4ClO_2^{\bullet}+5NaCl+2H_2O \quad (1\text{-}1)$$

$$ClO_2^{\bullet}+ h\upsilon \rightarrow Cl^{\bullet} + O_2 \quad (1\text{-}2)$$

Hence, in this study, PCL was chosen as the model polymer lacking side-chain methyl groups for surface oxidation and it was pressed into the film via hot pressing. The surface

modification process involved the utilization of light-activated $ClO_2^{\bullet}$ gas as an oxidizing reagent, which was facilitated by UV light irradiation. The investigation included an evaluation of the effects of the oxidation duration and illuminated UV light intensity on factors such as hydrophilicity, elemental ratios, chemical components, and morphology. Moreover, a dye test was performed to confirm the presence of carboxyl groups and elucidate the underlying mechanism. It should be noted that UV light is only required for the activation of $ClO_2^{\bullet}$ gas and is not necessary for the modification process of the plastic surface.[35] Consequently, for comparison, the PCL film was exclusively exposed to UV light. In addition, electroless metal plating was performed on an oxidized PCL film to explore its potential applications. This approach is anticipated to broaden the range of available materials suitable for polymer substrates coated with metal layers

1-2. Experimental section

Materials

High-molecular-weight PCL(M_n=80,000) and sodium chlorite ($NaClO_2$) were obtained from Sigma-Aldrich (Tokyo, Japan). Hydrochloric acid (HCl) (35%-37%), chloroform ($CHCl_3$) and pseudomonas lipase (PS) were purchased from Wako Pure Chemical Industries, LTD (Osaka, Japan). Chloroform-d ($CDCl_3$) was purchased from Thermo Fisher Scientific, Inc. (Osaka, Japan). Copper plating solutions (OPC-50 Inducer M, OPC-150 Crystal RW, and ATS Addcopper IW) were obtained from Okuno Chemical Industry (Osaka, Japan). All the reagents were used without further purification.

Preparation of PCL Film

PCL films were prepared by hot-pressing. The PCL particles were dried overnight in a freeze dryer before use. 8 g of Dried PCL particles were initially heated between the hot plates (inner size: 100 mm × 100 mm × 4.5 mm) in a pressing machine for 5 min at 80 °C until PCL particles completely melted. A hot-pressing plate was purchased from the Nilaco Corporation (Tokyo, Japan) and washed with $CHCl_3$ before use. Subsequently, the hot plates were pressed

at 5 Mpa for 5 min to prepare films. The hot plates were then cooled to room temperature to obtain the PCL films with thickness of 5 mm.

Oxidation of PCL Film

$ClO_2^{\bullet}$ gas was used as an effective oxidizing agent for the PCL film oxidation under ambient conditions. An aqueous solution was prepared by dissolving $NaClO_2$ (100 mg) and HCl (0.1 mL) in deionized water (7 mL) with magnetic stirring. The $ClO_2^{\bullet}$ gas was generated from the aqueous solution under UV light irradiation.[34-36]

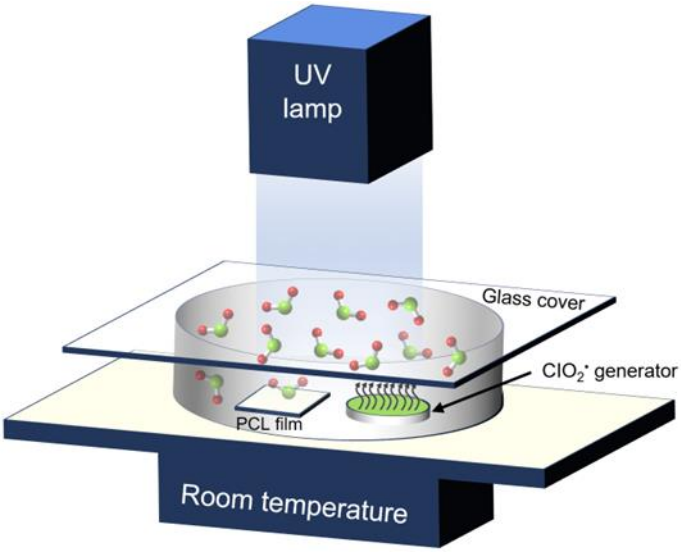

Figure 1-1. Schematic of oxidation process for PCL film.

$ClO_2^{\bullet}$ was photo-chemically activated by an UV lamp (HOLOLIGHT KAKU lamp, λ = 365 nm), to yield a $Cl^{\bullet}$ radical and oxygen. No chlorine gas was generated under these reaction conditions. The PCL film was cut into pieces 20 mm wide and 50 mm high and then placed in a petri dish with a diameter of 100 mm. Simultaneously, the aforementioned aqueous solution was prepared in a smaller petri dish with a diameter of 25 mm. The PCL film was oxidized using UV light-activated $ClO_2^{\bullet}$ gas under ambient gas conditions, and the oxidation system was covered with a glass plate to prevent gas leakage. To investigate the effect of varying oxidation degrees on the performance of PCL films, gas generation was regulated by adjusting both the intensity and duration of illumination. The illumination intensities of the reaction vessel were set to 15, 25, 35, 45, and 55 $mW \cdot cm^{-2}$ for comparison. The oxidation times were 10, 20, 30, 40, and 50 min, and the inner aqueous solution was replaced with fresh solution every 10 min. A schematic of this process is shown in **Figure 1-1**All samples were thoroughly rinsed with deionized water and subsequently dried in a vacuum drier at 25 °C before testing.

Characterization

Water contact angles were measured using a Drop Master DM 300 (Kyowa Interface Science, Saitama, Japan). The water contact angle was measured at 5 s after the contact with 0.5 μL of a water droplet and the value was calculated as the average of 5 different positions for each sample. The surface elemental composition was evaluated using X-ray photoelectron spectroscopy (XPS, JPS-9010MC, JEOL, Tokyo, Japan). The XPS parameters included the power of analysis (wide:75 W, narrow:150 W), monochromatic Al Kα. The survey and high-resolution XPS spectra were collected at fixed analyzer pass energies of 160 and 10 eV, respectively. The atomic concentrations of the elements were calculated using CasaXPS Version 2.3.25 (Casa Software LTD, Digital Data Management Corp., Chiba, Japan). Moreover, the integrated areas of the spectral lines and relative sensitivity factors quoted in the CasaXPS database were used to calculate the atomic concentrations of the elements. The chemical compositions and functional groups were determined by ATR-FTIR(FT/IR4500, JASCO) at room temperature with diamond window. All spectra were acquired at 4 cm^{-1} resolutions over 36 scans in the scan range of 500-4000 cm^{-1}. To confirm the reproducibility, the measurement was performed over 3 times for each sample. The morphology of the PCL film was observed by scanning electron microscopy (SEM, SU3500, Hitachi Co., Ltd., Tokyo, Japan) at 15 kV. All samples were sputtered with an Au-Pd layer using an E-1010 ion-sputtering apparatus (Hitachi, Tokyo, Japan) in advance. Microstructural changes and surface roughness were characterized using atomic force microscopy (AFM, Seiko Instruments Inc.). The roughness was calculated from the AFM images and presented as the root mean square (RMS) using Nanosurf easyscan2 software. Differential scanning calorimetry (DSC) and thermal gravimetric analysis (TGA) were carried out in an thermogravimetric analyzer (Hitachi, Tokyo, Japan). About 10 mg of samples were heated from 30 to 600, with the heating rate of 10 °C·min^{-1} under constant nitrogen flow (102 cm^3·min^{-1}) for TGA. DSC measurement was carried out from -100 °C to 80 °C at 10 °C/min under constant nitrogen flow. The tensile behavior of the samples was determined using a AGS-X type tensile tester (Shimadzu, Kyoto, Japan) at room temperature with a maximum speed of 5 mm/min and maximum force of 50 N. The chemical structure of the oxidized PCL film surface was determined by proton nuclear magnetic

resonance (^{1}H-NMR) spectroscopy using a JNM-ECS400 (400 MHz, JEOL Ltd., Tokyo, Japan) with $CDCl_3$ as the solvent. The molecular weight of the PCL film surface was measured by Gel Permeation Chromatography (GPC) using HLC-8420 GPC (Tosoh, Tokyo, Japan) with $CHCl_3$ as the solvent. Molecular weight was calculated with a calibration curve derived from polystyrene standards with $CHCl_3$ as the eluent flowing ratio at 0.5 $mL \cdot min^{-1}$ and a sample concentration of 10.0 $mg \cdot mL^{-1}$.

Enzymatic degradation

Enzymatic degradation of PCL films before and after oxidation was carried out at 25 °C and 37 °C in a 0.1 M Phosphate buffer (PH=7.0) solution containing lipase.[37] Each PCL film with initial weight of W_0 and dimension of 10 × 10 mm, was put into a small glass tube containing 10 mL of the buffer solution and 1 mg of lipase. The tube was incubated at 25 °C and 37 °C in a bioshaker (M/BR-022UP, Taitec, Ehime, Japan). The films were picked up periodically, washed with deionized water and dried until a constant weight (W_t) was achieved. The relationship between weight loss (Equation 1-3) and degradation time was investigated.

$$\text{Weight loss} = (W_0 - W_t)/W_0 \quad (1\text{-}3)$$

Dyeing Experiment

A solution of Toluidine Blue O (TBO) dye (0.5 mg) was prepared by dissolving TBO in deionized water in a plastic bottle and magnetically stirring for 3 h. Subsequently, both the unoxidized and oxidized PCL films were immersed in the TBO dye solution for 30 min. Subsequently, the films were removed and washed twice with deionized water and then immersed in a 50vt% acetic acid solution for 30 min for desorption. This adsorption-desorption cycle was repeated five times for the oxidized PCL film. To quantify the concentration of the TBO dye solution, a microplate reader (SH9000LAB; Corona Electric Co., Ltd., Ibaraki, Japan) was used at 630 nm. A standard solution of TBO at different concentrations was prepared to build a standard curve. Using this standard curve, the concentrations of the TBO solutions

before and after dye adsorption were determined. The adsorption capability was assessed based on the concentration disparity before and after adsorption.

Electroless Plating

Copper plating involves a two-step catalytic approach known as the sensitizing/activation method[34, 36]. The unoxidized and oxidized PCL films were subjected to this procedure. Initially, they were deposited into an OPC-50 Inducer M solution at a temperature of 45 °C for 6 min. The films were then carefully rinsed with deionized water to remove any residue.

Following the rinsing step, the PCL film was immersed into an OPC-150 Crystal RW solution at a temperature of 25 °C for 5 min. This stage is crucial for the subsequent Cu deposition process.

For the actual copper deposition, the films were immersed in an ATS ADDcopper IW solution at 25 °C for 5 min. This step facilitated the formation of a Cu layer on the film surface.

Finally, the copper-plated film underwent two cycles of washing with deionized water and was then dried using a vacuum drier. The integrity of the adhesion of the metal layer to the polymer film was evaluated using a Scotch®-tape adhesion test according to the standard ASTM D3359, which provided insights into the strength of the bond between the copper layer and the film.

1-3. Result and Discussion

Elemental Ratio and Chemical Component of PCL Film

To confirm the existence of polar groups, XPS was first employed on both the unoxidized and oxidized PCL films. The composition and proportions of elements within the PCL films were directly obtained from XPS surveys using the CasaXPS software, and the results are shown in **Figure 1-2(a), (b), and (c)**. Primarily, the surfaces of the PCL films were fundamentally composed of C1s and O1s peaks, reflecting the underlying chemistry. The PCL film retained its elemental composition after oxidation. The elemental ratio of C/O was 3.08 for the unoxidized PCL film aligned with the chemical structure of PCL ($(C_6H_{12}O_2)_n$). As the oxidation time increased, the C/O ratio progressively decreased, reaching 2.43 at an oxidation

time of 40 min (**Figure (b)**). This decline in the C/O ratio was correlated with the introduction of additional polar groups onto the surface of the film owing to oxidation. This result is under a previous report on polymers with methyl groups in side chain.[34-36] Prolonged contact between the film surface and radical gas facilitated improved oxidation. Nevertheless, in the case of excessive oxidation, such as at the oxidation time of 50 min, the C/O ratio exhibited an unexpected increase. It was speculated that this phenomenon was attributed to the appearance of surface cracks as the oxidation progressed, which was confirmed by SEM and discussed in later. Radical-gas-induced cleavage of chemical chains during oxidation leads to the formation of smaller, more easily detachable segments. Consequently, during the washing steps, these small segments were released, revealing the unoxidized inner portions and causing an elevation in the C/O ratio.

Similar tendency can be observed by increasing UV intensity, as shown in **Figure 1-2(c)**, the C/O ratio reached 2.37 with an increase in light intensity to 45 $mW \cdot cm^{-2}$. Similarly, an increase in the ratio occurred with an excessively high UV intensity. This indicates that oxidation effect can be improved by increasing the UV light intensity and oxidation time. From these results, it can be inferred that an optimal oxidation outcome can be achieved using certain parameters. To prevent surface release and the associated increase in C/O ratio, it is advisable for the oxidation time to remain below 40 min and the UV intensity to remain weaker than 45 $mW \cdot cm^{-2}$. This approach ensures the maintenance of the desired surface chemistry and properties.

The chemical component ratios were determined from curve fitting of the high-resolution C1s spectrum from the XPS results, as shown in **Figure 1-2(d)**. The C1s curve exhibited three discernible peaks at 285.0 eV, 286.5 eV, and 288.0 eV, which were attributed to C-O, C-O/C-OH, and C=O/C=OH, respectively.[38] The absence of new peaks indicates minimal alteration in the chemical structure, indicating relative stability. The sum ratio of the oxygen-containing functional groups on the PCL film surface before oxidation was approximately 25 % (**Figure 1-2(e)**). When the oxidation time reached 40 min, the oxygen-containing ratio increased to a maximum (30%). Remarkably, no significant difference was found in the polar group ratio, which agrees with the elemental ratio results.

Furthermore, the effect of varying the UV light intensity on the chemical component ratio was investigated, as shown in **Figure 1-2(f)**. Notably, the sum of oxygen-containing components exhibited saturation as the light intensity increased to 45 mW·cm^{-2}. It can be inferred that a comparable effect on the oxidation process was achieved with the oxidation time and UV light intensity.

XPS results revealed the introduction of polar groups onto the surface of PCL film by chlorine dioxide radical gas. With prolonged oxidation time and increased light intensity, the presence of polar groups exhibited a discernible upward trajectory, which is consistent with the findings from literature on the oxidation of polymers featuring methyl groups. [34-36] Notably, PCL lacks methyl groups, which typically serve as sites for oxidation into hydroxyl or carboxyl groups. In addition, the excessive oxidation time and light intensity may result in a reduction in

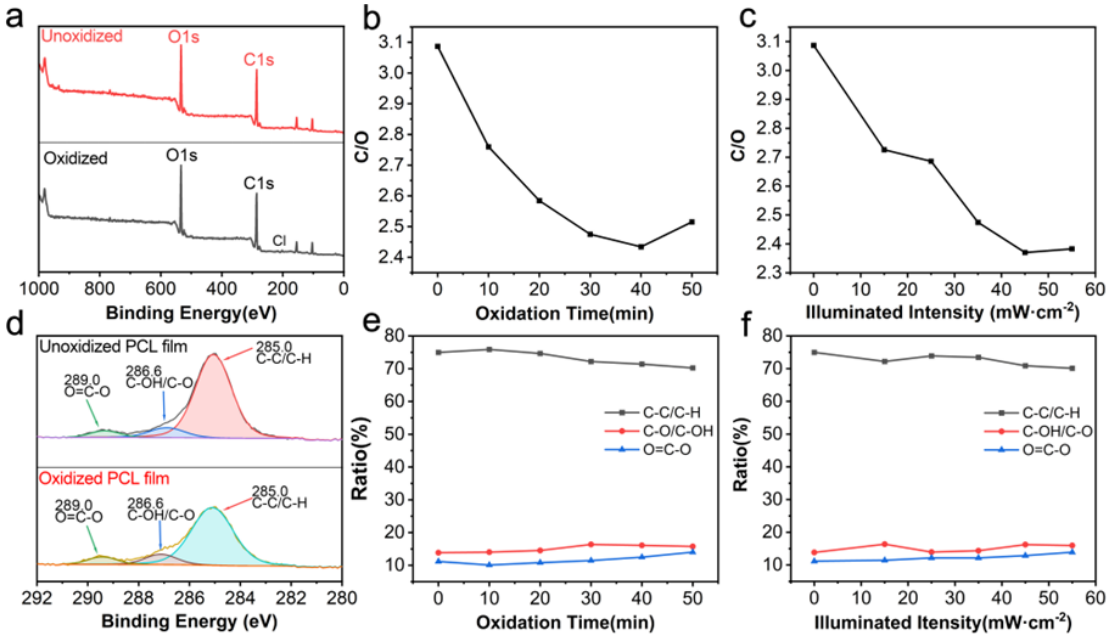

Figure 1-2. XPS result of PCL film. (a) Survey curves of unoxidized and oxidized PCL film. (b) Elemental ratio of C/O on surface of PCL film under different illuminated intensities with oxidation time of 30 min. (c) Elemental ratio of C/O on surface of PCL film with different oxidation times under illuminated intensity of 35mW·cm^{-2}. (d) C1s spectra of unoxidized and oxidized PCL film. (e) Chemical component ratios of C-C/C-H, C-OH/C-O and O=C-O on surface of PCL film under different illuminated intensities with oxidation time of 30 min. (f) Chemical component ratios on surface of PCL film with different oxidation times under illuminated intensity of 35mW·cm^{-2}

the proportion of polar groups. These phenomena will be subjected to further analysis in later chapters.

Hydrophilicity of PCL Film

Water contact angle measurements were employed to assess the hydrophilicity of both unoxidized and oxidized PCL films. As shown in **Figure 1-3(a)**, the water contact angle value of the unoxidized PCL film was 99.1°±1.1°, attributed to the inherent hydrophobicity nature of PCL. After oxidation, a noticeable reduction in the water contact angle was observed, with the value decreasing as oxidation time increased. Notably, upon reaching an oxidation time of 50 min, the water contact angle value dropped to approximately 66.2°±5.7°, making a shift from a hydrophobic to a hydrophilic characteristic in the PCL film (**Figure 1-3(c)**).

This transformation is related to the introduction of polar groups, such as -COOH and -OH, onto the film surface**.** These hydrophilic groups on the surface of the PCL film make it easier to form hydrogen bonds with water molecules, thus increasing the surface energy.[39] This behavior arose from an elongated interaction period between the film surface and the radical gas as the oxidation time increased, resulting in heightened ratios of polar groups. Thus, the water contact angle decreased with increasing oxidation time.

The effect of the UV illumination intensity on the oxidation process and hydrophilicity is shown in **Figure 1-3(b)**. As the illuminated UV intensity escalated, the water contact angle exhibited a corresponding reduction, reaching its minimum at light intensity of 45 mW·cm^{-2} with a value of 75.4±3.4°. The UV illumination

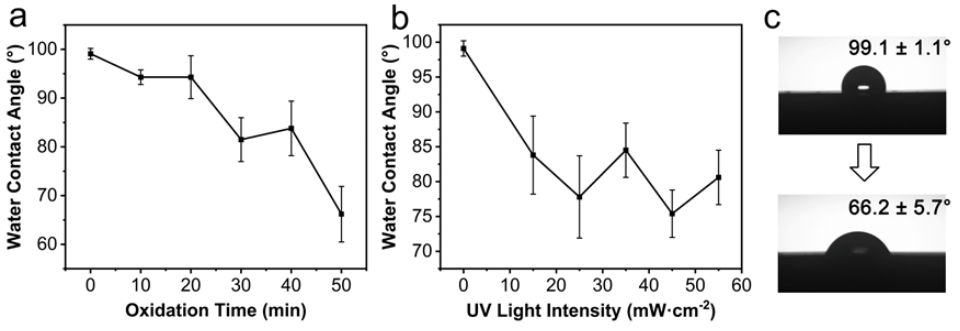

Figure 1-3. Water contact angle of PCL film with (a) different oxidation time under UV light of 45 mW·cm^{-2} and (b) different UV light intensity with oxidation time of 40 min. (c) Photograph of water contact angle before and after oxidation.

intensity directly affects the rate of radical gas production. Lower intensities translated to sluggish radical gas production rates, resulting in limited contact between the film surface and the radical gas. This, in turn, leads to a protracted oxidation reaction

With an increase in intensity, the pace of radical gas production accelerates, augmenting the concentration of radical gas in the glass watch. This increased concentration facilitates oxidation interactions between the film and the radical gas, ultimately boosting the presence of polar groups on the film surface. Thus, the hydrophilicity of the film was improved. Compared to other surface modification methods applied to PCL-based materials,[40-43] the surface oxidation method demonstrated a considerable improvement effect in hydrophilicity. **(Table 1-1)**

A similar effect can be achieved by increasing the UV light intensity or prolonging the oxidation time. Hence, focusing solely on the effect of the oxidation time on the PCL film properties, the subsequent sections delve into this aspect in greater detail.

Table 1-1. Water contact angle value of PCL after surface oxidation with different methods.

Methods	Water contact angle(°)	reference
Laser surface modification	60	[40]
Sodium hydroxide surface treatment	61	[41]
Ultraviolet ozone treatment	69	[42]
Plasma treatment	50	[43]
Surface oxidation	66	This work

Morphology of unoxidized and Oxidized PCL Film

Scanning electron microscopy (SEM) was used to verify the alteration in surface morphology due to oxidation. As shown in **Figure 1-4**, the surface roughness of the PCL film increases after oxidation, with the effect becoming particularly pronounced at extended oxidation times (**Figure 1-4(e)** and **(f)**). Notably, in the case of excessively prolonged oxidation time, discernible cracks emerged on the film surface, as shown in **Figure 1-4(f)**. The augmentation of surface roughness has implications for hydrophilicity because a rougher

surface is commonly associated with enhanced hydrophilic attributes of materials of this nature. This observation is consistent with the results of water contact angle regarding water contact angle. As the oxidation process continued, the chemical chains of PCL underwent sessions and shortening, leading to deterioration of its mechanical properties. Consequently, the transition from a pliable to a brittle state renders it more susceptible to cracking.

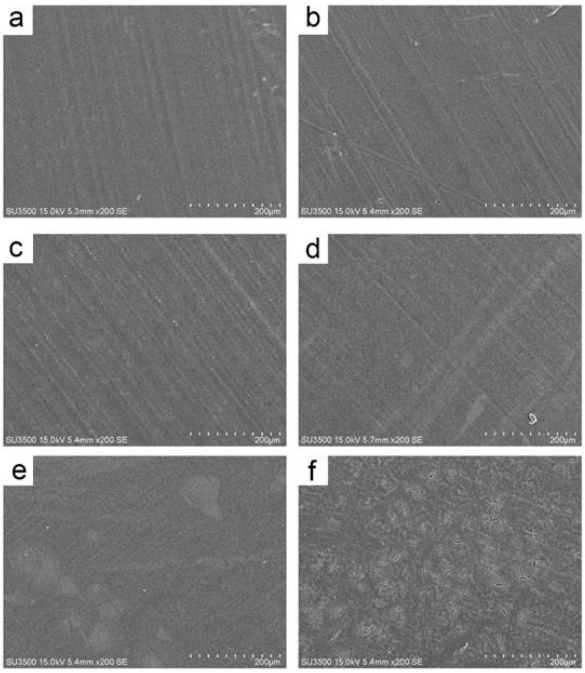

Figure 1-4. SEM images of (a) unoxidized PCL film and oxidized PCL films with oxidation time of (b) 10 min, (c) 20 min, (d) 30 min, (e) 40 min, and (f) 50 min under illuminated intensity of 45 mW·cm^{-2}.

To further study the changes in surface roughness before and after oxidation, AFM images were obtained, as shown in **Figure 1-5**. After oxidation, a discernible increase in roughness was observed, with the RMS value increased from 8.83 nm to 16.94 nm. This trend was consistent with the observations from the SEM images. Moreover, as the oxidation time increased, the surface roughness continued to increase, eventually reaching an RMS value of 20.88 nm at an oxidation time of 40 min. The surface of the unoxidized PCL displayed a degree of roughness owing to the presence of the mold release reagent. The hot-pressing

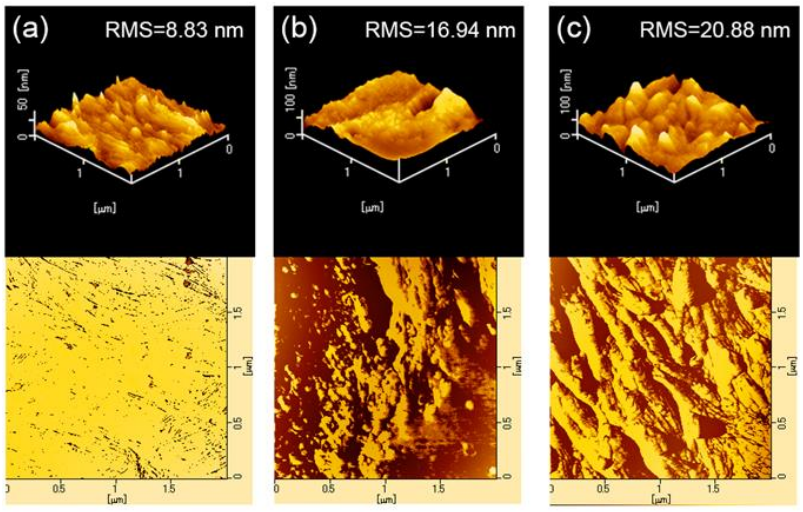

Figure 1-5. AFM images of (a) unoxidized PCL film and oxidized PCL film with oxidation time of (b) 20 min and (c) 40 min.

method resulted in a smooth film surface with a residual release reagent. Following washing with ethanol, the release agent on the surface was removed, increasing the surface roughness. Upon surface oxidation by radical gases, the roughness experienced a slightly modest increase. Importantly, the increased roughness has the potential to bolster the adhesion capability[44] and improve the hydrophilicity of the PCL films. These attributes hold significant value for the practical applications of these materials.

Exploring 25 different conditions for surface oxidation, a comprehensive analysis revealed the optimal parameters for PCL film oxidation: an ideal oxidation time of 40 minutes and an illuminated light intensity of 45 $mW \cdot cm^{-2}$. These specific conditions yielded a substantial number of oxygen-containing groups on the surface, effectively enhancing the surface properties without inducing damage.

Enzymatic degradation

Degradation property of PCL film after oxidation was evaluated at 25°C and 37°C, with the results presented in **Figure 1-6**. It can be seen that oxidized PCL film retained its biodegradability, with increased degradation rates observed at both temperatures. It is speculated that the improvement in degradation rate can be attributed to the improvement in hydrophilicity, facilitating the action of enzyme-containing solution on the surface of film.[45,46] In addition, the higher surface roughness of the oxidized PCL film is also conducive to the attachment of enzymes.

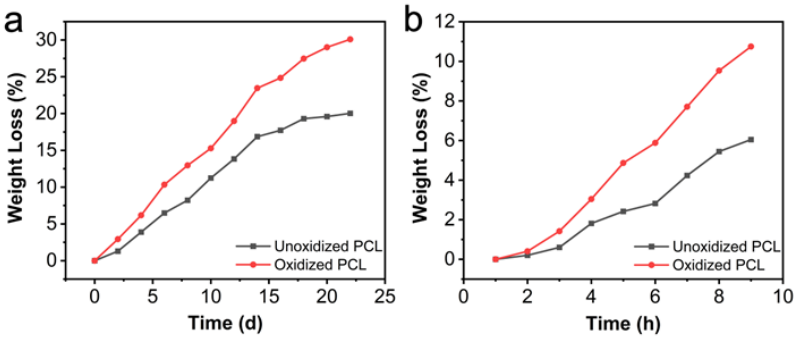

Figure 1-6. Weight loss of unoxidized and oxidized PCL films after enzymatic degradation by lipasePS at (a) 25 °C and (b) 37 °C.

Oxidation Mechanism

To study the oxidation mechanism and the chemical structure before and after oxidation, the ^{1}H NMR was first used. There are 3 main peaks observed (**Figure 1-7(a)**) at distinct chemical shifts: δ_a=4.01-4.06 ppm (C<u>H</u>$_2$-OCO), δ_b=2.26-2.33 ppm (C<u>H</u>$_2$-COO), δ_c=1.57-1.65 ppm (C<u>H</u>$_2$-CH$_2$-O and C<u>H</u>$_2$-CH$_2$-COO), and δ_d=1.29-1.49 ppm (CH$_2$-C<u>H</u>$_2$-CH$_2$), which were same with the ^{1}H-NMR result of PCL with other's work. [47] Moreover, the peak at δ=4.6 ppm is attributed to the hydroxyl proton at the end of the PCL chain, and δ=3.6 ppm belongs to methylene protons bound to the hydroxyl group (-CH$_2$-OH) and can only be observed at the oxidized PCL spectrum. The ratios of the end groups increased after oxidation because the main chains of PCL were cut by the radical gas during the oxidation process. This phenomenon can be attributed to the cleavage of the main chains within PCL caused by the radical gas during the oxidation process. Chain scission results from the robust oxidizing properties of radical gas. Furthermore, the molecular weight of the oxidized PCL film surface decreased by these structural changes, as detected by GPC.

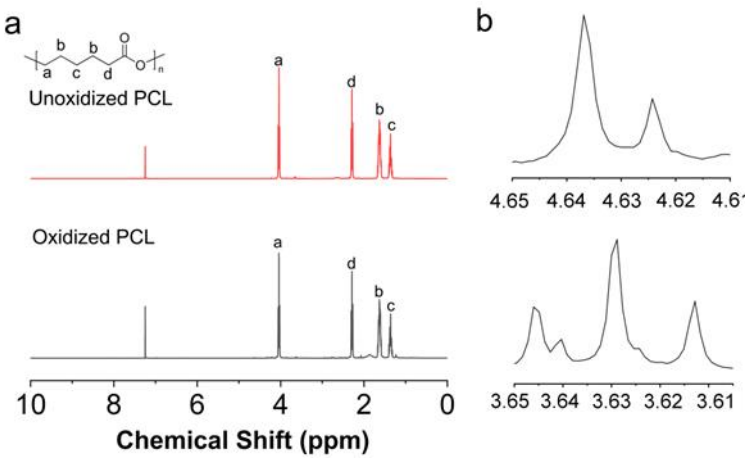

Figure 1-7. (a) ^{1}H-NMR spectra of unoxidized PCL and oxidized PCL film surface. (b) High-resolution ^{1}H-NMR spectra of oxidized PCL film at chemical shift of δ=3.6 ppm and δ=4.6 ppm.

The GPC data were processed using specialized software (Ecos Elite WS). The number-average molecular weight (M_n), weight-average molecular weight (M_w), and polydispersity index (PDI) are presented in **Table 1-2**. The GPC curves exhibited an unimodal symmetric distribution, and the M_w of PCL decreased from 151,788 to 17,317 after oxidation. Correspondingly, the PDI increased from 2.1 to 3.7 after oxidation. This implies that the oxidation process led to the cleavage of the PCL molecules on the surface of the film by the radical gas from the ester groups. Consequently, the ratios of the hydroxyl and carboxyl groups

increased, whereas the chemical structure remained stable. Additionally, the nonuniformity of the chain scission reaction led to an increase in the PDI value.

Table 1-2. Molecular weight of PCL films before and after oxidation under different conditions

Oxidation conditions	M_n	M_w	PDI
45 mW·cm^{-2}, 0 min	70743	151788	2.146
45 mW·cm^{-2}, 20 min	8319	53136	6.387
45 mW·cm^{-2}, 40 min	4703	17317	3.682
without $NaClO_2$ solution	68231	141640	2.076

A controlled experiment was designed to determine the effects of UV light alone, excluding the presence of a radical gas-generating solution. A comparison between the unoxidized PCL film and the PCL film exposed solely to UV light showed negligible differences in M_n, M_w, and PDI. This result indicates that the radical gas, and not the UV light, acted as the driving force behind the chain scission reaction and surface oxidation process.

Drawing from the results of the characterization measurements, the feasible mechanism in this study involved Cl• radicals reacting with PCL to generate various oxygen-containing functional groups on the surface. The PCL surface underwent chain scission, forming free radical intermediates, which subsequently transferred to terminal hydroxyl and carboxyl groups with the help of water molecules present in the air. **Figure 1-8** illustrates possible reactions.

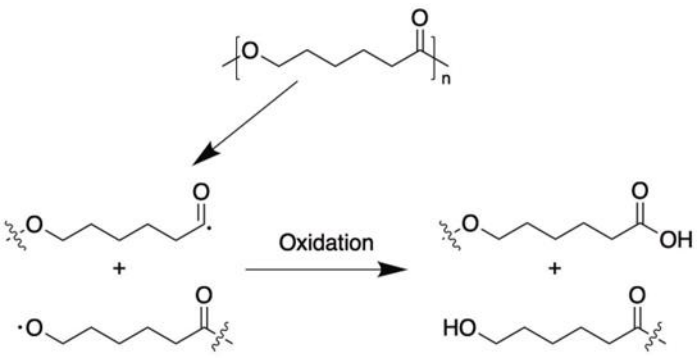

Figure 1-8. Possible oxidation mechanism of PCL film surface by photo-irradiated ClO_2•.

TBO Adsorption Experiment

The TBO type, which is known for its ability to interact with -COOH groups in polymers through hydrogen bonding, was chosen for the adsorption experiment to confirm the presence of -COOH groups. This bond was destroyed using a 50% acetic acid solution. As shown in **Figure 1-9(a)**, the oxidized PCL film was dyed blue by the TBO solution after 30 min, whereas the unoxidized PCL film retained its original color. Subsequent treatment with a 50vt% acetic acid solution for 30 min reversed the color change, and the dyed PCL film returned to its initial color.

For precise quantification, the concentration of the TBO solution was assessed using a microplate reader at an absorbance of 630 nm, and the corresponding standard curve is graphically presented in **Figure 1-9(b)**. Following 30 min adsorption, the concentration of TBO solution decreased from 0.5 mg/L to approximately 0.25 mg/L. The adsorption capacity was calculated using Equation 1-4:

$$Q = (C-C_0)V/W \quad (1\text{-}4)$$

where Q is the adsorption capacity of the adsorbent. C and C_0 are the final and initial concentrations of the TBO solution, respectively. V is the volume of the dye solution, and W is the weight of the sample.

To confirm the reusability of the samples, five adsorption and desorption cycles were carried out. As shown in **Figure 1-9(c)**, the concentration decreased from 0.5 mg/L to 0.25 mg/L after adsorbed by oxidized

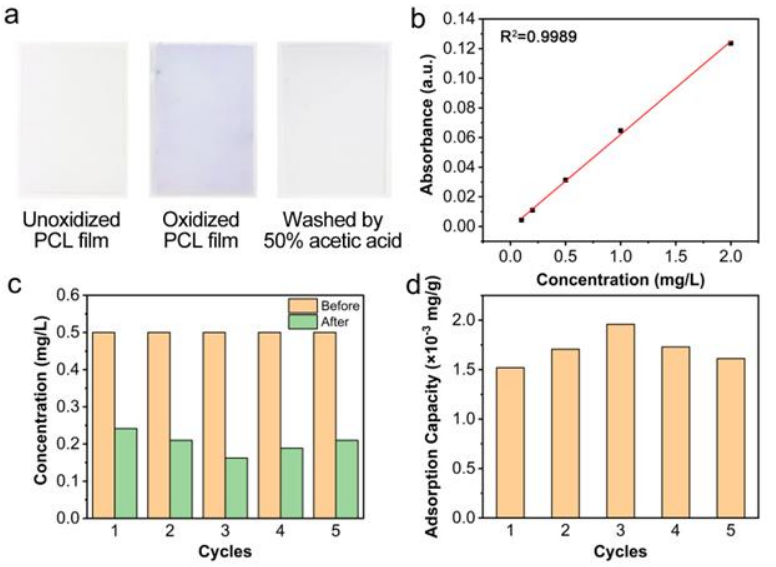

Figure 1-9. TBO dye adsorption result. (a) Picture of PCL films dyed with 50vt% TBO solution and washed with 50vt% acetic acid. (b) The calibration curve of TBO aqueous solution. (c) The concentration of TBO solution before and after 5 cycles of adsorption by oxidized PCL film. (d) Adsorption capacity calculated from (c).

PCL film after 30 min. According to formula (3), it can be calculated that the adsorption capacity was approximately $1.5*10^{-3}$ ~ $2.0*10^{-3}$ mg/g (**Figure 1-9(d)**). After washing with a 50vt% acetic acid solution, the sample was reused for another adsorption experiment with minimal alteration in its adsorption capacity.

Electroless Plating

Both the unoxidized and oxidized PCL films were deposited into a sensitizer/activator solution and then immersed in a copper plating solution, as shown in **Figure 1-10(a)**. The OPC-50 catalyzed copper plating, while OPC-150 was employed for activating the catalyst. Initial parameters were established based on the literature reports,[34,36] and the optimal conditions for PCL were refined through multiple attempts. Following immersion in a Cu^{2+} solution (ATS Addcopper IW) for 5 min, both unoxidized and oxidized PCL films were completely plated with a copper layer. The adhesion strength is a significant parameter, and good adhesion properties between polymer matrix and metal layer can provide the corrosion resistance and service life. Qualitative analysis of adhesion property was conducted using a Scotch®-tape adhesion test. **Figure 1-10(a)** shows that the copper layer on the surface of the unoxidized PCL film is completely removed after the tape test. In contrast, superior adhesion between the oxidized PCL film and the copper layer was observed. The adhesion of the oxidized PCL film surface to the copper layer was enhanced by the introduction of polar groups onto the surface. This interaction facilitated a more favorable interaction between the loaded catalyst of Pd^{2+} and the polar groups,

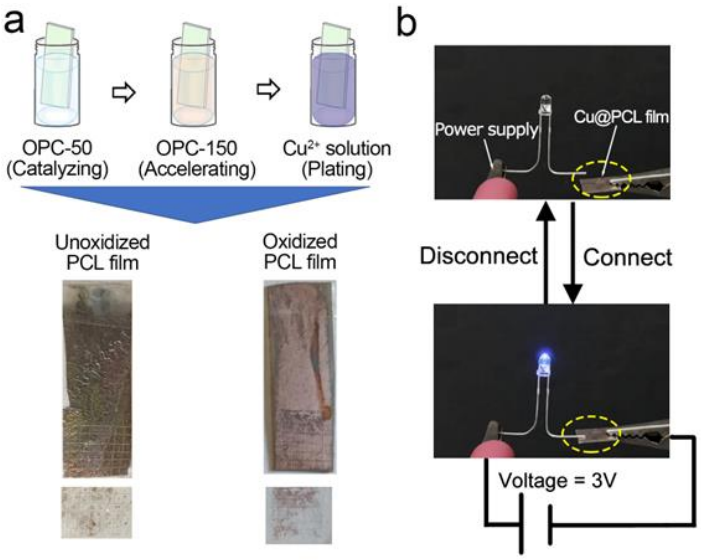

Figure 1-10. (a) Schematic diagram and tape test result of copper plating process for unoxidized and oxidized PCL film. (b) Pictures of conductivity test of copper plated PCL film with and without power.

thereby resulting in a higher plating efficiency. Additionally, improved surface roughness contributes to the effectiveness of the metal plating process. It was indicated that the light-activated $ClO_2^{\bullet}$ surface oxidation method is an efficient method for the application of pretreatment of metal plating for PCL based materials.

Subsequently, a conductivity experiment was conducted on the copper-plated PCL film using an LED lamp. As shown in **Figure 1-10(b)**, the LED lamp was illuminated upon establishing contact with the copper-plated film powered by the setup. It was proven that the copper layer possessed a measurable thickness and impressive electrical conductivity. The copper-plated PCL film exhibits promising potential for application as a multi-functional material.

1-4. Conclusions

The surface modification of the PCL film was successfully achieved via oxidation using light-activated $ClO_2^{\bullet}$ gas. Successful oxidation was confirmed by XPS. Oxygen-containing functional groups were introduced onto the surface of the PCL film, resulting in an increased oxygen ratio and oxygen-containing components after oxidation. A reduction of the water contact angle from 99.1°±1.1° to 66.2°±5.7° was observed, indicating the transformation of PCL film from hydrophobic to hydrophilic. Optimal oxidation conditions were determined as the oxidation time of 40 min and illuminated UV light intensity of 45 $mW \cdot cm^{-2}$ for the PCL film. Exceeding these conditions led to a diminishing oxygen ratio, and an excessively high light intensity and prolonged oxidation time caused the emergence of surface cracks. These cracks not only compromise the mechanical properties, but also affect their potential applications.

The oxidation mechanism was inferred through ^{1}H-NMR and GPC measurements, which indicated the scission of PCL molecules on the surface of the film into smaller segments via radical gases from the ester groups. This resulted in elevated levels of hydroxyl and carboxyl groups at the ends of the fragments. Importantly, because only a thin surface layer underwent oxidation, the material integrity remained intact. Concurrently, enhancements were observed in tensile strength, crystallinity properties and degradation performance.

The oxidized PCL film exhibited good adsorption capability for the TBO dye solution and can be expected to be applied for dye wastewater treatment. Owing to the presence of carboxyl groups, the oxidized PCL film could be dyed using the TBO solution, in contrast to the unoxidized film.

Additionally, electroless copper plating demonstrated successful copper deposition on both unoxidized and oxidized PCL films, with more robust bonding observed between the oxidized PCL and the copper layer. This underscores the possibility of a straightforward $ClO_2^{\bullet}$ gas-based surface oxidation method as a potential avenue for enhancing PCL materials. Furthermore, a comprehensive optimization scheme for polymer-metal coatings is proposed, offering a pathway towards the realization of multi-functional polymers.

1-5. References

[1] Zhang, X.; Fan, W.; Liu, T. *Compos. Commun.*, **2020**, *21*, 100413.

[2] Abeykoon, C.; Sri-Amphorn, P.; Fernando, A. *Int. J. Lightweight Mater. Manuf.*, **2020**, *3* (3), 284–297.

[3] Maqsood, N.; Rimašauskas, M. *Compos. Part C: Open Access*, **2021**, *4*, 100112.

[4] Bamiduro, O.; Owolabi, G.; Haile, M. A.; Riddick, J. C. *RPJ*, **2019**, *25* (3), 462–472. https://doi.org/10.1108/RPJ-04-2018-0087.

[5] Rosso, S.; Meneghello, R.; Biasetto, L.; Grigolato, L.; Concheri, G.; Savio, G. *Addit. Manuf.*, **2020**, *36*, 101713.

[6] Zheng, W.; Wu, J.-M.; Chen, S.; Yu, K.-B.; Hua, S.-B.; Li, C.-H.; Zhang, J.-X.; Shi, Y.-S. *Addit. Manuf.*, **2021**, *48*, 102396.

[7] Gu, H.; Bashir, Z.; Yang, L. *Addit. Manuf.*, **2019**, *28*, 194–204.

[8] Gui, C.; Yao, C.; Huang, J.; Chen, Z.; Yang, G. *Appl. Surf. Sci.*, **2020**, *506*, 144935.

[9] Huang, J.; Xu, L.; Zhao, D.; Wang, J.; Chu, C.; Chen, H.; Liu, Y.; Chen, Z. *Chem. Eng. J.*, **2020**, *383*, 123199.

[10] Shacham-Diamand, Y.; Osaka, T.; Okinaka, Y.; Sugiyama, A.; Dubin, V. 30 *Microelectron. Eng.*, **2015**, *132*, 35–45.

[11] Mallory, G. O.; Hajdu, J. B. *Electroless Plating: Fundamentals and Applications*; William Andrew, 1990.

[12] Zhu, C.; Li, T.; Mohideen, M. M.; Hu, P.; Gupta, R.; Ramakrishna, S.; Liu, Y. *Polymers*, **2021**, *13* (5), 744.

[13] Dethe, M. R.; A, P.; Ahmed, H.; Agrawal, M.; Roy, U.; Alexander, A. *J. Control. Release*, **2022**, *343*, 217–236.

[14] Singh, S.; Alrobaian, M. M.; Molugulu, N.; Agrawal, N.; Numan, A.; Kesharwani, P. *ACS Omega*, **2020**, *5* (21), 11935–11945.

[15] Mulchandani, N.; Masutani, K.; Kumar, S.; Yamane, H.; Sakurai, S.; Kimura, Y.; Katiyar, V. *Polym. Chem.*, **2021**, *12* (26), 3806–3824.

[16] Sommer, K.; Van Opdenbosch, D.; Zollfrank, C. *Polymers*, **2023**, *15* (2), 455.

[17] Liu, L.; Wang, S.; Qi, P.; Song, S.; Yang, Y.; Shi, J.; Han, G. *Int. J. Pharm.*, **2020**, *590*, 119885.

[18] Háková, M.; Havlíková, L. C.; Chvojka, J.; Erben, J.; Solich, P.; Švec, F.; Šatínský, D. *Microchim. Acta.*, **2019**, *186* (11), 710.

[19] Moosavi, M. H.; Khani, M. R.; Shokri, B.; Hosseini, S. M.; Shojaee-Aliabadi, S.; Mirmoghtadaie, L. *Int. J. Biol. Macromol.* **2020**, *142*, 769–777.

[20] Lin, P. C.; Lin, K. F.; Chiu, C.; Semenov, V. I.; Lin, H. C.; Chen, M. J. *Surf. Coat. Technol.*, **2021**, *427*, 127811.

[21] Wong, L.-W.; Loke, X.-J.; Chang, C.-K.; Ko, W.-C.; Hou, C.-Y.; Hsieh, C.-W. *Food Chem.*, **2020**, *329*, 126989.

[22] Stankevičius, E.; Ignatjev, I.; Petrikaitė, V.; Selskis, A.; Niaura, G. *ACS Omega*, **2021**, *6* (49), 33889–33898.

[23] Kotsedi, L.; Furlan, V.; Bharadwaj, V.; Kaviyarasu, K.; Sotillo, B.; Mtshali, C. B.; Matinise, N.; Demir, A. G.; Previtali, B.; Ramponi, R.; Eaton, S. M.; Maaza, M. *Opt. Mater.*, **2019**, *95*, 109206.

[24] Ries, R.; Seiler, E.; Gömöry, F.; Medvids, A.; Onufrijevs, P.; Pira, C.; Chyhyrynets, E.; Malyshev, O. B.; Valizadeh, R. *Supercond. Sci. Technol.*, **2021**, *34* (6), 065001.

[25] Deng, L.; Li, S.; Qin, Y.; Zhang, L.; Chen, H.; Chang, Z.; Hu, Y. *J. Membr. Sci.*, **2021**, *619*, 118564.

[26] Zhang, G.; Wang, T.; Xu, Z.; Liu, M.; Shen, C.; Meng, Q. *Chem. Commun.*, **2020**, *56* (76), 11283–11286.

[27] Gu, Q.; Ng, T. C. A.; Zain, I.; Liu, X.; Zhang, L.; Zhang, Z.; Lyu, Z.; He, Z.; Ng, H. Y.; Wang, J. *Appl. Surf. Sci.*, **2020**, *502*, 144128.

[28] Pitchayya Pillai, G.; Manimaran, P.; Vignesh, V. *J.Nat. Fibers*, **2021**, *18* (12), 2102–2111.

[29] Ganapathy, T.; Sathiskumar, R.; Senthamaraikannan, P.; Saravanakumar, S. S.; Khan, A. *Int. J.Biol. Macromol.*, **2019**, *138*, 573–581.

[30] Mukhtar, I.; Leman, Z.; Zainudin, E. S.; Ishak, M. R. *J. Nat. Fibers*, **2020**, *17* (6), 877–889.

[31] Brennan, W. J.; Feast, W. J.; Munro, H. S.; Walker, S. A. *Polymer*, **1991**, *32* (8), 1527–1530.

[32] Yaghoubi, H.; Taghavinia, N. *Appl. Surf. Sci.*, **2011**, *257* (23), 9836–9839.

[33] Ohkubo, K.; Hirose, K. *Angew. Chem. Int. Ed.*, **2018**, *57* (8), 2126–2129.

[34] Jia, Y.; Asahara, H.; Hsu, Y.-I.; Asoh, T.-A.; Uyama, H. *Appl. Surf. Sci.*, **2020**, *530*, 147202.

[35] Jia, Y.; Chen, J.; Asahara, H.; Asoh, T.-A.; Uyama, H. *ACS Appl. Polym. Mater.*, **2019**, *1* (12), 3452–3458.

[36] Jia, Y.; Wu, W.; Asahara, H.; Hsu, Y.-I.; Asoh, T.-A.; Tan, H. T.; Sudesh, K.; Uyama, H. *Polym. Degrad. Stab.*, **2021**, *191*, 109661.

[37] Gan Z, Liang Q, Zhang J, et al. *Polym. degrad.stab.*, 1997, 56(2): 209-213.

[38] Briggs D. Surface analysis of polymers by XPS and static SIMS. *Cambridge University Press*, Cambridge, 1998.

[39] Shikata, T.; Okuzono, M. *J. Phys. Chem. B*, **2013**, *117* (25), 7718–7723.

[40] Tiaw KS, Goh SW, Hong M, et al. *Biomaterials*, 2005, 26(7): 763-769.

[41] Wang W, Caetano G, Ambler W S, et al. *Materials*, **2016**, 9(12): 992.

[42] Samsudin N, Hashim YZHY, Arifin MA, et al. *Cytotechnology*, **2017**, 69: 601-616.

[43] Sousa I, Mendes A, Pereira R F, et al. *Mater. Lett.*, **2014**, 134: 263-267.

[44] Zou, M.; Beckford, S.; Wei, R.; Ellis, C.; Hatton, G.; Miller, M. A. *Appl. Surf. Sci.*, 2011, 257 (8), 3786–3792.

[45] Gazvoda L, Višić B, Spreitzer M, et al. *Polymers*, **2021**, 13(11): 1719.

[46] Place E S, George J H, Williams C K, et al. *Chem. soc. rev.*, **2009**, 38(4): 1139-1151.

[47] Bagheri, M.; Mahmoodzadeh, A. *J. Inorg. Organomet. Polym.*, **2020**, 30 (5), 1566–1577.

Chapter 2

Development of a Flow Reactor Incorporating Polydopamine-Poly(ε-caprolactone) with Gold Particles

2-1. Introduction

Water is an essential resource on earth, sustaining life and providing habitats for marine organisms. However, due to the development of industrialization, water was seriously polluted. The relentless march of industrialization has led to severe water pollution. Of particular concern is the prevalence of dyes in wastewater, originating from diverse industrial sectors such as textiles, paper manufacturing, and paints. Hence, the treatment of dye-contaminated water effluent has emerged as one of the most challenging tasks concerning the concern of the environmental fraternity.

Dyes commonly divided into natural and synthetic dyes, refer to organic compounds that can make other substances obtain bright and steady colors. [1] The emergence of synthetic dyes since 1869, spurred by diversified production methods, gradually supplanted many natural alternatives due to their cost-effectiveness. [2] Today, the array of synthetic dyes surpasses 100,000 types, with azo dyes emerging as the most prevalent, constituting over 70% of global dye production. [1] The widespread usage of azo dyes inevitably results in the substantial discharge of dye wastewater, which accounts for more than half of the world's total wastewater output, making it the primary contributor to global wastewater pollution. [3] Compounding this issue is the inherent toxicity of many synthetic dyes, posing significant environmental risks. [4,5] Addressing the removal of these toxic substances from wastewater is paramount for mitigating environmental degradation and safeguarding aquatic ecosystems.

Various physicochemical and biological methods have been applied for the removal of azo dye from water, including precipitation and coagulation [6,7], membrane filter, [8,9] adsorption [10,11] and catalytic degradation [12,13]. However, some of these methods suffer from the problems such as low efficiency and secondary pollution. Among them, catalytic degradation stands out as an efficient approach for wastewater pollutant removal without causing secondary pollution. Precious metal particles are the most frequently used catalysts, such as Au, Ag, Pt, Pd, due to

their large surface area to volume ratios. [14–16] In particular, Au particles have demonstrated significant efficacy in degrading azo dyes. [17–21] However, the agglomeration of Au particles can lead to a reduction in catalytic efficiency due to the decreased contact area with substrate. Moreover, considering their small size and high cost, methods for recycling Au particles are essential to mitigate precious metal pollution and ensure economic viability. In this context, the choice of catalyst carrier becomes crucial for practical application. Supported Au particles have shown promising potential in the degradation of azo dyes, yet literature documenting such findings remains limited. [22]

Porous materials are fundamental components in various applications, serving as alternative catalyst carriers. Among them, monoliths have emerged as novel porous materials since the 1990s. [23] They possess distinctive features such as a 3D interconnected pore structure, substantial surface area, and customizable sizes, rendering them suitable for continuous processes such as adsorption, [24,25] separation, [26,27] and catalyst carriers [28,29]. Polymer-based monoliths have garnered significant interest due to their low density and robust stability, particularly in harsh chemical environments such as acidic or alkaline conditions.

In pursuit of eco-friendly development and to combat plastic pollution, biodegradable polymers have gained widespread adoption in recent years. Notable examples include PLA, poly(vinyl alcohol), and PCL. Among these, PCL stands out as a cost-effective biodegradable polymer that can naturally degrade in both environmental and biological settings, owing to the presence of ester groups in its main chain. However, the high hydrophobicity of PCL presents challenges for its utilization in wastewater treatment. Consequently, there is an urgent need for surface modification of PCL-based materials to enhance their functionality and applicability, particularly in the field of wastewater treatment.

In this study, PCL was selected as the matrix polymer to fabricate the porous monolith via N-TIPS method. A solvent mixture of 1,4-dioxane and ethanol was employed, with ethanol serving as the non-solvent instead of water as commonly found in literature [30,31] This substitution significantly reduced the consumption of 1,4-dioxane from over 70% to less than 30%, resulting in cost savings and minimizing organic solvent usage, thereby mitigating potential environmental pollution. Surface modification was carried out using PDA due to its

inherent adhesion properties. PDA's catechol groups acted as a reducing agent to convert Au^{3+} to Au. [32] Additionally, PDA's adhesive properties facilitated the immobilization of Au particles onto the surface of the PDA-PCL monolith. Catalytic experiments conducted using MO, a common azo dye found in wastewater, yielded promising results, demonstrating the effective catalytic capability and reusability of the Au-immobilized PDA-PCL monolith (Au@PDA-PCL monolith).

2-2. Experimental section

Materials

3 types of PCL with different molecular weights (PCL_1 M_n=10,000, PCL_2 M_n=42,500, PCL_3 M_n=80,000) were commercially obtained from Sigma-Aldrich Co. LLC (St Louis, MO, USA). 1,4-dioxane was purchased from Nacalai Tesque Inc. (Japan). Dopamine hydrochloride was purchased from Lkt Laboratories Inc. (Minnesota, USA). Deionized water was prepared from Mili-Q system from Millipore Corp. (Milford, MA, USA). Tris-HCl buffer (pH=8.5) was purchased from Nippon Gene Co., Ltd. (Tokyo, Japan). Hydrogen tetrachloroaurate(III) tetrahydrate, MO and sodium borohydride ($NaBH_4$) were purchased from Fujifilm Wako Pure Chemical Corp. (Osaka, Japan). All reagents were used without further purification.

Fabrication of PCL monolith

The fabrication process of the PCL monolith followed our previous work via N-TIPS method. [33] Briefly, a solvent mixture of 1,4-dioxane and ethanol was prepared in a glass tube and heated at 60 ℃. A certain amount of PCL particles was dissolved into the solvent mixture and stirred magnetically for 4 hours until a transparent and homogeneous PCL solution was obtained. After that, the glass tube was transferred to 4 °C condition for 24 hours to induce complete phase separation, then wet PCL monolith would be obtained consequently. The organic solvent in PCL monolith was exchanged with deionized water using a bio-shaker for 24 hours, with the deionized water changed every 4 hours. PCL monolith was obtained after drying with a vacuum dryer. While previous studies extensively investigated parameters such as polymer concentration, solvent ratio, and phase separation temperature, this study focused

on evaluating the impact of polymer molecular weight on PCL monolith fabrication using three common commercial products. Detailed process parameters are provided in **Table 2-1**.

Table 2-1. Process parameters of PCL monolith fabrication

Sample	M_n	PCL concentration (g/L)	Solvent ratio ($V_{1,4\text{-dioxane}}/V_{ethanol}$)
PCL_1 monolith	10000	100	75/25
PCL_2 monolith	42500	100	75/25
PCL_3 monolith	80000	100	75/25

Fabrication of PDA-PCL monolith

The fabrication of PDA-PCL monolith involved a self-polymerization reaction of dopamine (DA). [34] Briefly, DA solution was prepared by dissolving 0.1 g of dopamine hydrochloride in 50 mL of Tris-HCl buffer (pH = 8.5). Subsequently, 20 mL of ethanol was added into the DA solution to facilitate its penetration throughout the porous structure of the PCL monolith. To ensure optimal coating, the upper and bottom sides of PCL monolith were cut down before immersion in the DA solution for 24 hours with magnetic stirring. During this process, the PCL monolith and DA solution underwent a color change from colorless to dark indicative of PDA formation through self-polymerization of DA in the presence of air. Then, the PDA-PCL monolith was washed with deionized water for 2 days, with water changed every 4 hours, and then dried using a vacuum dryer.

Fabrication of Au@PDA-PCL monolith

A PDA-PCL monolith was fixed into the heat shrinkable tube for Au immobilization. The monolith underwent pre-treatment with liquid nitrogen to preserve its morphology. Immobilization was achieved using a peristaltic pump. An aqueous solution of $HAuCl_4 \cdot 4H_2O$, with a concentration of 10 mg/mL was prepared and pumped through the monolith for 3 hours to facilitate the formation of Au particles through the reduction of PDA. [35] After that, the solution was changed to deionized water and pumped for another 30 min to wash the prepared

Au@PDA-PCL monolith.

Characterization

Differential scanning calorimetry (DSC) was carried out in a thermogravimetric analyzer (Hitachi, Tokyo, Japan) from 0 °C to 70 °C under constant nitrogen flow. The morphologies of samples were observed by a scanning electron microscope (SEM, SU3500, Hitachi Co., Tokyo, Japan) at 15 kV. Surface elemental compositions were evaluated by Energy Dispersive Spectrometer (EDS) and X-ray photoelectron spectroscopy (XPS; JPS-9010MC, JEOL, Tokyo, Japan). The atomic concentrations of elements were calculated using the CasaXPS Version 2.3.22 computer program (Casa Software LTD, Digital Data Management Corp., Chiba, Japan). Moreover, an integrated area of spectrum lines and relative sensitivity factors quoted in the CasaXPS database were used for calculating the atomic concentrations of elements.

Calculation of immobilization capacity

The immobilization capacity of Au was calculated by equation (2-1).

$$C=V(c_1-c_2)/M \quad (2\text{-}1)$$

where the C is the immobilization capacity. c_1 and c_2 are the Au^{3+} concentrations before and after immobilization in the $HAuCl_4 \cdot 4H_2O$ aqueous solution. V is the volume of the Au^{3+} aqueous solution and M is the weight of PDA-PCL monolith carrier. The Au^{3+} concentration in the solution was determined by UV-vis Absorption Spectroscopy based on the standard curve of Au^{3+}, which was determined with the pre-prepared solution with the concentration of 40, 60, 80, 100 and 120 mg/L. Since the absorption peak of Au^{3+} would shift with pH, to get an accurate standard curve, the pH of every solution was adjusted to 1 with hydrochloric acid in advance.

Catalytic experiment

MO was selected as the dye model because of its common usage in the textile industry and its suitability for monitoring via UV-vis spectroscopy. For the catalytic evaluation, 40 mL of MO aqueous solution was prepared at a concentration of 20 mg/L, supplemented with 0.05 mol/L $NaBH_4$ as the reducing agent. The MO solution was pumped through the Au@PDA-PCL

monolith using a peristaltic pump at a flow rate of 2.5 mL/min. The effluent was collected and analyzed using UV-vis spectroscopy. The catalytic efficiency was determined by measuring the concentration difference before and after catalysis as equation (2-2).

$$E = (c_0\text{-}c)/c_0 \quad (2\text{-}2)$$

Where E is the catalytic efficient. c_0 and c are the concentrations of the initial dye solution and effluent solution. To assess the reusability of Au@PDA-PCL monolith, the catalytic experiment was repeated for 5 cycles at a flow rate of 2.5 mL/min, with 40 mL of aforementioned MO solution utilized for each cycle. After each cycle, the monolith was washed with deionized water to remove any residual compounds.

As a comparison, the catalytic degradation experiment was also conducted using a batch method. The Au@PDA-PCL monolith was directly immersed in 40 mL of aforementioned MO solution for the degradation process. 0.5 mL of MO solution was taken out every 5 min for concentration measurement.

2-3. Result and discussion

TIPS process of PCL monolith

The crystalline temperature (T_c) is a crucial parameter in N-TIPS process, as it is typically recognized as the beginning of solid-liquid (S-L) de-mixing process and serves as the ending point of phase separation. DSC was therefore employed to measure the T_c of PCL with different molecular weights, and the result is shown in **Figure 2-1(a)**. The curves exhibited similar trends, indicating consistent crystallization behavior among PCL particles with different molecular weights. The T_c was approximately 25℃

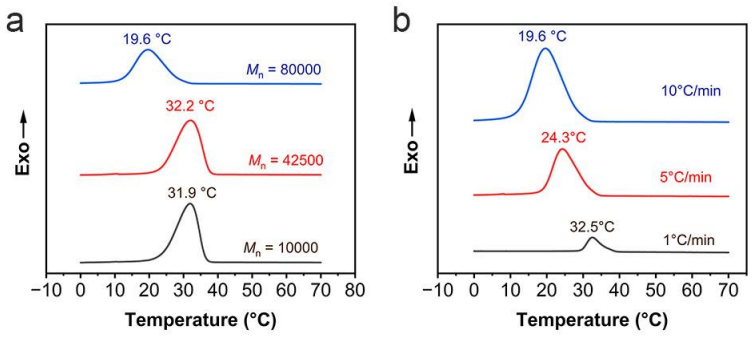

Figure 2-1. DSC plots of PCL. (a) A cooling scan of PCL particles with 3 types of molecular weight from 70 ℃ to 0 ℃ with cooling rate of 10 ℃/min. (b) A cooling scan of PCL_3 particles from 70 ℃ to 0 ℃ with different cooling rates.

and tended to move to a lower temperature with the increase of PCL molecular weight. The increase in molecular weight leads to the length growth of molecular chain, which impedes the movement of chain segments, resulting in a decrease of the crystallization temperature. [36] On the other hand, T_c point was found to be significantly influenced by the cooling rate, as illustrated in **Figure 2-1(b)**. It was observed that the T_c shifted to a higher temperature position as the cooling rate decreased. As reported in the literature, this variation is attributed to the intrinsic non-isothermal crystallization process of PCL, which leads to the development of imperfect crystals at higher cooling rates. [37,38]

The phase separation process of PCL solution with different molecular weights was greatly influenced by T_c. When the PCL solution was cooled to 4℃ for phase separation, only PCL_3 monolith could be successfully formed. This was because of the difficulty in conducting the S-L de-mixing process in PCL_1 and PCL_2 solutions compared to PCL_3. The narrow temperature gradient between solving temperature and T_c leads to insufficient liquid-liquid (L-L) demixing time, resulting in an incomplete phase separation process. Furthermore, during the cooling process, the gradual narrowing of the temperature gradient between the solution's internal temperature and the external temperature led to a reduction in the cooling rate. This gradual decrease in cooling rate favored the formation of monoliths, particularly for PCL_3, where the extended liquid-liquid demixing time facilitated monolith formation. It is demonstrated that the higher molecular weight or lowered setting temperature of phase separation are important factors as they play pivotal roles in determining the success of phase separation.

Based on these results, PCL_3 was chosen for the preparation and discussion of the PDA-PCL monolith for following tests.

Surface modification by PDA

The effectiveness of PDA coating was initially confirmed by EDS analysis with the results presented in **Table 2-2**. In the EDS analysis of the PCL monolith, only carbon (C) and oxygen (O) elements were detected, consistent with the composition of PCL. After coating with PDA, an additional 17% nitrogen (N) content was observed in the EDS result of PDA-PCL monolith. It was indicated that the N-containing components adhered to the surface of the monolith,

validating the successful coating with PDA.

The XPS analysis was performed to characterize the surface composition and quantify the amount of PDA on the surface of PDA-PCL monolith. The survey spectra are presented in **Figure 2-2(a)**. Compared to the spectrum of PCL monolith, an additional peak of N 1s between 397 eV and 402 eV was observed in the PDA-PCL monolith, by which the existence of PDA was proved once again. Quantitative analysis of the elemental composition was performed using CapaXPS software, with the result summarized in **Table 2-3**. The analysis revealed that 5.29% and 2.14% of N were detected on the exterior and interior surfaces of PDA-PCL monolith, respectively. This discrepancy in nitrogen content can be attributed to the fact that the self-polymerization of DA in the air. Consequently, the exterior surface of the monolith, being in direct contact with oxygen, exhibits a higher nitrogen content compared to the interior surface.

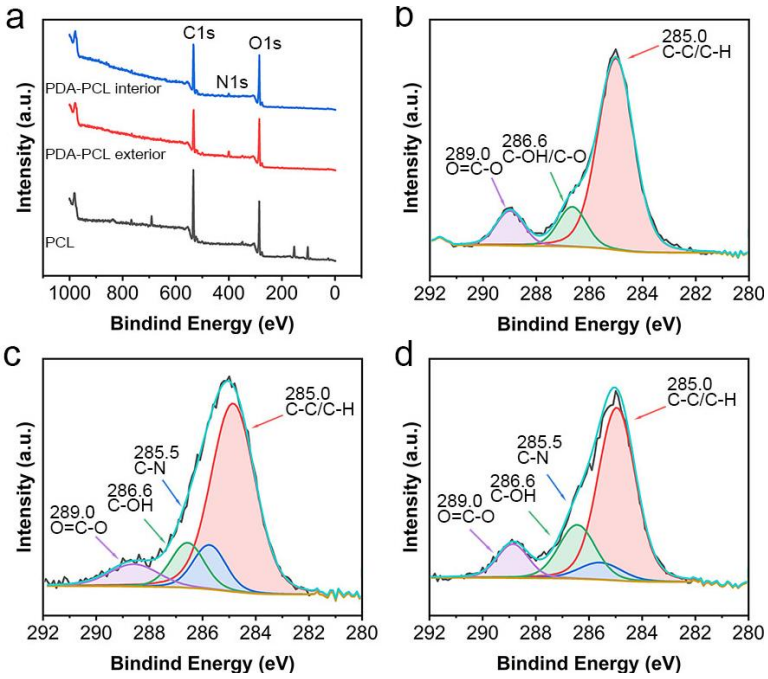

Figure 2-2. XPS spectra of PCL and PDA-PCL monolith. (a) Survey, (b)C1s of PCL monolith. (c)C1s of exterior of PDA-PCL monolith. (d) C1s of interior of PDA-PCL monolith.

To further investigate the chemical components of the PCL and PDA-PCL monolith, C 1s obtained from the survey and its peak fitting were presented in **Figure 2(b-d)**. The peaks observed at binding energies of 285.0 eV, 286.6 eV, and 289 eV corresponded to C-C/C-H, C-O and O-C=O, respectively. [39] Following the coating with PDA, an additional peak assigned to C-N at 285.5 eV appeared. The amount of C-N was determined to be 11.71% and 7.47% on the exterior and interior surfaces, respectively.

These results demonstrated that PDA was coated on the surface of PCL monolith successfully, and the PDA can be remained after washing.

Table 2-2. The element concentration of PCL monolith and PDA-PCL monolith determined from EDS result

Element	Weight concentration (%)		Atomic concentration (%)	
	PCL monolith	PDA-PCL monolith	PCL monolith	PDA-PCL monolith
C	66.15	48.45	72.24	54.40
N		17.94		17.28
O	33.85	33.60	27.76	28.32

Table 2-3 Element ratios obtained from XPS surveys

	C	O	N	C-C/C-H	C-N	C-OH	O=C-O
PCL	72.70	27.30		74.87		13.24	9.96
PDA-PCL exterior	72.60	22.11	5.29	67.16	11.71	12.12	9.00
PDA-PCL interior	73.40	24.45	2.14	61.79	7.45	20.08	10.69

Au immobilization

To ensure effective immobilization, a peristaltic pump was employed to facilitate the passage of the Au^{3+} solution through the PDA-PCL monolith. During this process, the sample was fixed in a heat shrinkable tube and then connected to the pump.

The existence of Au particles was confirmed by XRD with the XRD patterns of PDA-PCL monolith and Au@PDA-PCL monolith (**Figure 2-3**). The XRD pattern of the PCL monolith revealed significant crystallinity, characteristic of semi-crystalline polymers, with peaks observed at 21.9° and 24.2° corresponding to the (110) and (200)

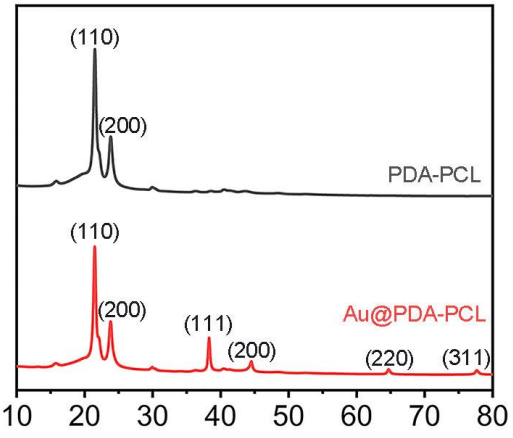

Figure 2-3. XRD patterns of PDA-PCL monolith and Au@PDA-PCL monolith.

planes of the orthorhombic crystal structure. [40] Following modification with PDA, the XRD curve remained stable, as PDA itself does not crystallize. upon immobilization of Au particles, new peaks emerged at 38.3°, 44.7°, 64.6°, and 77.8° in the XRD pattern of the Au@PDA-PCL monolith. These peaks correspond to the (111), (200), (220), and (311) planes, indicative of the crystalline nature of the Au particles with a face-centered cubic (fcc) structure. The XRD results confirm the successful immobilization of Au particles on the surface of the PDA-PCL monolith, demonstrating the ability of PDA to act as a reducing agent for the conversion of Au^{3+} to particles.

The efficacy of immobilization was further validated through EDS analysis with the results shown in **Table 2-4**. Notably, the presence of Au peaks was evident in the Au@PDA-PCL monolith, accounting for approximately 5% of the total composition.

Table 2-4. Element concentration of Au@PDA-PCL monolith determined from EDS result

Element	Weight concentration (%)	Atomic concentration (%)
C	46.36	55.92
N	14.68	15.19
O	31.28	28.33
Au	7.68	0.57

The XPS spectra and quantitative analysis of Au@PDA-PCL monolith are shown in **Figure 2-4** and summarized in **Table 2-5**. Quantitative analysis revealed the Au content on the exterior and interior surfaces to be 1.33% and 0.33%, respectively. This discrepancy in Au content can be attributed to the higher concentration of PDA and greater accessibility to Au^{3+} on the exterior surface. Consequently, the reaction between PDA and Au^{3+} is facilitated, resulting in a higher Au content on the exterior surface compared to the interior. Interestingly, a corresponding decrease in the N content was observed with an increase in the Au ratio. This phenomenon can be attributed to the reaction between PDA and Au^{3+}. During the Au immobilization process, PDA serves as a reducing agent, facilitating the reduction of Au^{3+} to Au particles. [41] Consequently, as the reaction progresses, the N content decreases, leading to a

reduction in the N ratio.

The ratios of each chemical component were calculated from C1s (**Figure 2-4(b)(c)**) and the results were presented in **Table 2-5**. It is worth noting that a decrease in the C-H and C-OH components was observed following immobilization, accompanied by an increase in O=C-O. This shift in chemical composition could be attributed to the involvement of the catechol group in PDA during the immobilization process. The catechol group acts as an oxidizing agent, facilitating the reduction of Au^{3+} to Au particles. [32] Consequently, it is speculated that the observed changes in chemical components may stem from the consumption of catechol structures during this reduction reaction. Simultaneously, the proportion of O=C-O structures within the PCL matrix increased.

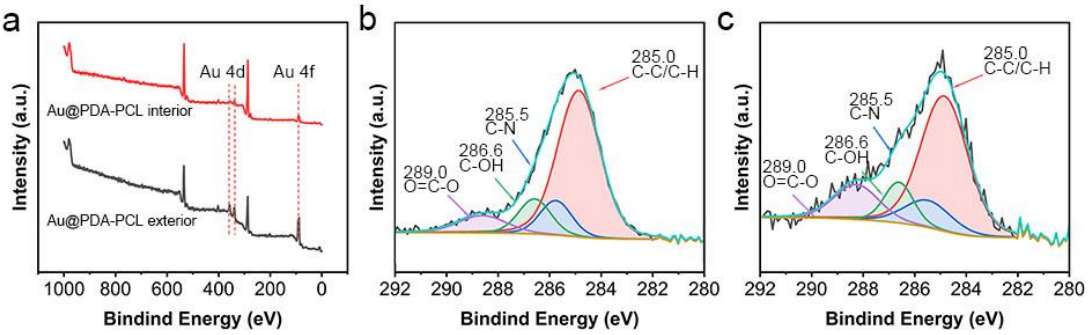

Figure 2-4. XPS spectra of Au@PDA-PCL monolith. (a) Survey, (b) C1s of interior. (c) C1s of exterior

Table 2-5. Element ratios obtained from XPS surveys and chemical components calculated from C 1s spectra.

	C	O	N	Au	C-C/C-H	C-N	C-OH	O=C-O
Au@PDA-PCL exterior	68.35	24.72	5.59	1.33	63.05	10.34	11.49	15.12
Au@PDA-PCL interior	74.44	23.81	1.42	0.33	59.30	8.97	18.34	13.39

Calculation of Au amount

The amount of Au immobilized on the surface of the PDA-PCL monolith was determined

based on the initial and final concentrations of Au^{3+} in the $HAuCl_4 \cdot 4H_2O$ monitored using UV-vis spectroscopy at a wavelength of 312 nm under pH=1 conditions (**Figure 2-5b**). A standard curve depicting the relationship between Au^{3+} concentration and absorbance intensity was established (**Figure 2-5a** inset). Following immobilization for 4 hours, the Au^{3+} concentration decreased from 10 mg/mL to 5.88 mg/mL. Considering a prepared volume of 40 mL of Au^{3+} solution, it was deduced that 164.8 mg of Au particles were immobilized on the surface of 580 mg PCL. Thus, the immobilization efficiency was calculated to be 28.41 g/g. It is important to note that a minor loss of Au may have occurred during the transfer process; therefore, the actual content may be slightly lower than the calculated value.

These results confirm the successful reduction of Au^{3+} ions to Au particles and their immobilization on the surface of the PDA-PCL monolith. Furthermore, the adhesion properties of PDA ensured that the Au remained even after the washing process, thus endowing the Au@PDA-PCL monolith with significant potential for catalytic applications.

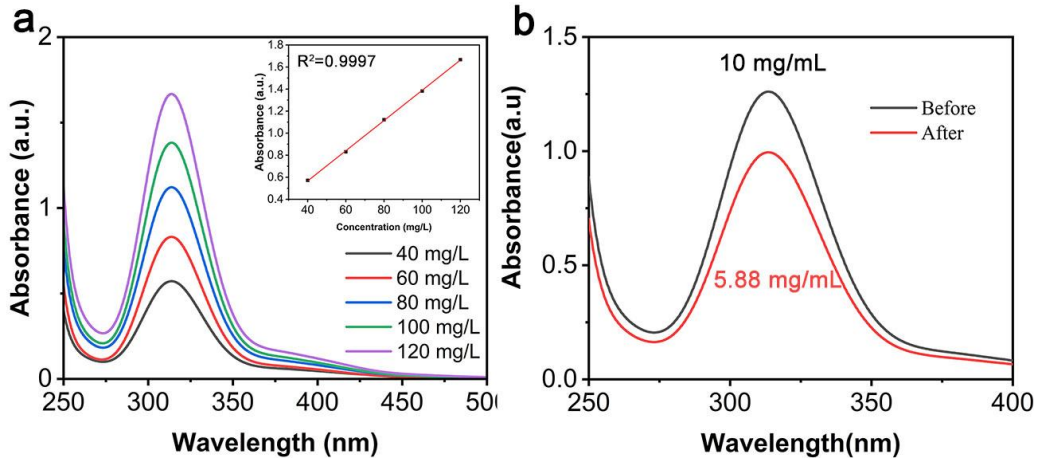

Figure 2-5. (a) Standard curve of Au^{3+} in $HAuCl_4 \cdot 4H_2O$ solution determined by UV-vis spectra. (b) UV-vis spectra of $HAuCl_4 \cdot 4H_2O$ solution before and after immobilization (spectra of diluting 100 times).

Catalytic degradation of MO

MO is an extensively used azo dye in various pharmaceuticals and textile industries but is cancerogenic. [42] Thus, its degradation to less toxic substances are significant before released to water. In this study, the reduction reaction of MO with $NaBH_4$ was selected as a model to assess the catalytic performance. UV-vis spectroscopy was employed to evaluate the catalytic

activity of MO degradation.

As shown in **Figure 2-6(a)**, the UV-vis spectrum of MO exhibits two characteristic peaks at 464 nm and 272 nm, corresponding to the azo absorbance peak and benzene ring charge transfer adsorption peak, respectively. [43] Since environmental pollution is primarily attributed to the azo group, the azo absorbance peak was utilized to calculate the MO concentration. A methyl orange standard curve was generated from the UV-vis spectra, as presented in **Figure 2-6(b)**.

For the catalytic process by batch method, it can be observed from **Figure 2-6(c)** that the absorbance peak of azo groups at 464 nm decreased within 5 min and nearly disappeared within 10 min of degradation, accompanied by a color change in the MO solution from yellow to colorless. After 5 min of catalysis, the catalytic efficiency reached 79.25%, and reached the maximum value of 98.66% after 15 min (**Figure 2-6(d)**). It is worth noting that a new peak appeared at 268 nm after degradation, which is the characteristic absorbance of *N*,*N*-dimethylaniline. [17] As shown in the schematic illustration of MO degradation in **Figure 2-7**, MO is firstly decomposed into intermediate products to complete decolorization, and the reaction rate is relatively fast. Then, the intermediate products continue to decompose into inorganic substances such as CO_2 or fatty acids. [44] It was proved that the Au@PDA-PCL monolith retained the catalytic activity of Au particles, demonstrating high catalytic efficiency for MO degradation.

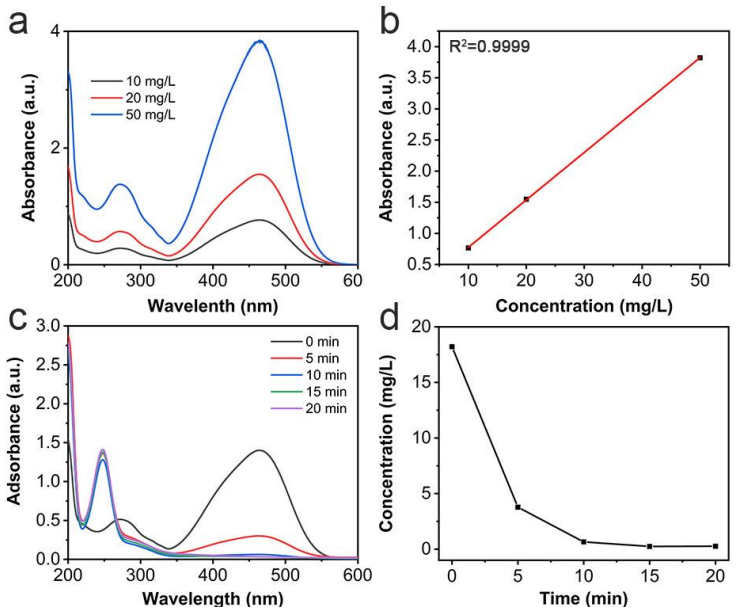

Figure 2-6. (a) UV-vis spectra of MO solution with different concentrations. (b) Standard curve of MO solution. (c) UV-vis spectra of MO dye solution with different degradation times. (d) The concentration of MO in dye solution at different times with the initial concentration of 18 mg/L.

The results of catalytic degradation with flow method are shown in **Figure 2-8**. After being pumped through the monolith with the flow rate of 2.5 mg/mL, the azo peak disappeared and the catalytic efficiency was calculated as 98.54%, as shown in **Figure 2-8(c)**. The stable and high catalytic efficiency can be achieved with various flow rates from 1.0 mL/min to 2.5 mL/min. However, a decline was observed beyond 2.5 mL/min. It was considered that excessively high flow rates limited the participation of Au particles in the reaction, resulting in reduced efficiency. Compared to the batch method, the use of a peristaltic pump facilitated enhanced contact between the solution and the Au particles within the interior pore structure of the monolith, which improved the contact area between the catalyst and the reactants, culminating in efficient catalysis within a shorter time. Furthermore, in comparison to other methods documented in the literature (**Table 2-6**), the results of this study showcase a notably higher degradation efficiency.

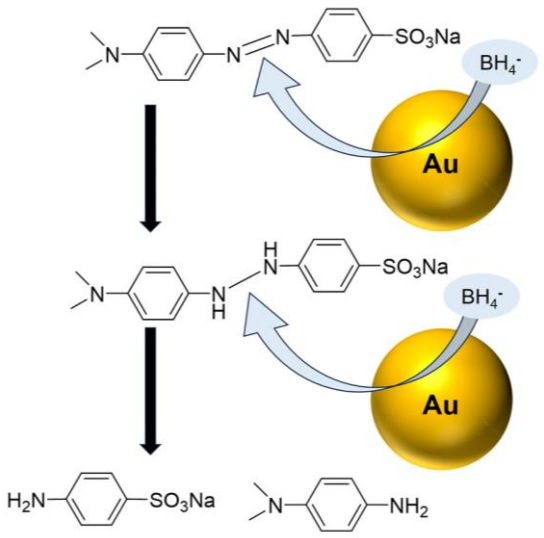

Figure 2-7. (a) Schematic illustration of degradation of MO in the presence of Au@PDA-PCL monolith

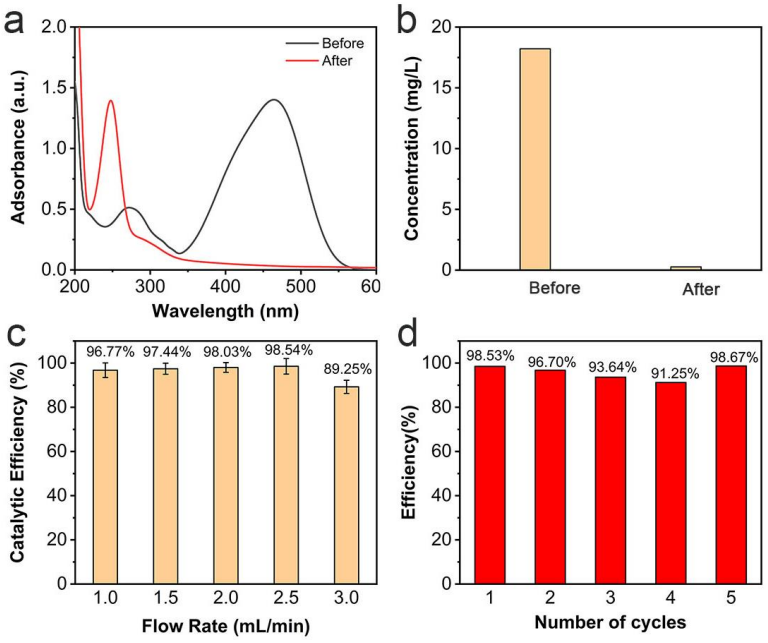

Figure 2-8. UV-vis spectra (a) and concentration (b) of MO solution before and after catalytic degradation using flow method. (c) Catalytic efficiency with different flow rates. (d) Reusability of Au@PDA-PCL monolith with the flow rate of 2.5 mL/min for 5 cycles.

[45-51]

The reusability of the catalyst was assessed by conducting repeated catalytic experiments on MO using the same catalyst sample at a flow rate of 2.5 mL/min. As depicted in **Figure 2-8(d)**, even after being recycled 5 times, the sample consistently exhibited a catalytic efficiency of over 90%. This underscores the excellent reusability of the Au@PDA-PCL monolith, highlighting its potential for practical applications.

Table 2-6. Degradation efficiency of MO with different methods.

Degradation method	Degradation efficiency	Reference
Catalytic degradation	98.5%	This work
Photocatalysis	95.0%	[45]
Ultrasound remediation	80.0%	[46]
Photocatalysis	91.5%	[47]
UV irradiation	96.9%	[48]
Peroxide oxidation	99.4%	[49]
Electrochemical oxidation	93.0%	[50]
Plasma oxidation	94.1%	[51]

2-4. Conclusions

An effective catalytic reactor was successfully fabricated as the format of Au@PDA-PCL monolith in this work. Firstly, the effect of molecular weight and cooling rate on N-TIPS process was discussed. It was found that higher molecular weight and lower cooling rate can improve the crystallization temperature of PCL, thereby increasing the end temperature of N-TIPS, so that the temperature requirement for phase separation is reduced.

PDA was used for surface modification of PCL monolith to improve the hydrophilicity of PCL monolith, permitting its further application in aqueous solution. At the same time, the PDA was used as a reducing agent to reduce Au^{3+} to Au particles and acted as a double tape to immobilize the Au particles on the surface of PDA-PCL monolith. XPS and EDS results show that both DA and Au particles exhibit a uniform distribution.

MO, which is a typical pollutant in dye wastewater, were selected as the dye model for catalytic degradation experiment. Au@PDA-PCL monolith fixed in heat shrinkable tube was employed for catalytic degradation with a peristaltic pump. This reactor showed the highest catalytic efficiency of 98.54%, resulting in a transition of MO solution from yellow color to colorless. In contrast to the batch method, the flow method offers a shorter catalytic time, ensuring more complete contact between Au particles and the MO solution, thereby resulting in higher efficiency for MO degradation What's more, the catalytic reactor showed a good reusability, and the catalytic efficiency didn't show significant decrease after 5 cycles.

2-5. References

[1] Y. Chen, F. Chen, L. Li, C. Su, B. Song, H. Zhang, S. Guo, F. Pan, *J. Magnes. Alloys.* 2024.

[2] A. Paz, J. Carballo, M.J. Pérez, J.M. Domínguez, *Chemosphere*. 2017, 181, 168.

[3] V. Selvaraj, T. Swarna Karthika, C. Mansiya, M. Alagar, *J. Mol. Struct*., 2021, 1224, 129195.

[4] H. Alhassani, M. Rauf, S. Ashraf, *Dyes and Pigments*, 2007, 75, 395.

[5] K. Golka, S. Kopps, Z.W. Myslak, *Toxicol. Lett.*, 2024, 151, 203.

[6] S. Zhao, B. Gao, Q. Yue, Y. Wang, *Colloids Surf. A: Physicochem. Eng. Asp.*, 2014, 456, 253.

[7] J.P. Dhal, M. Sethi, B.G. Mishra, G. Hota, *Mater. Lett.*, 2015, 141, 267.

[8] N. Ghaemi, S.S. Madaeni, P. Daraei, H. Rajabi, T. Shojaeimehr, F. Rahimpour, B. Shirvani, *J. Hazard. Mater.*, 2015, 298, 111.

[9] S. Zhao, Z. Wang, *J. Membr. Sci.*, 2017, 524, 214.

[10] S. Raja, A.K. Kola, D. Balakrishnan, T. Arunachalam, N. Rajarathinam, *Appl. Nanosci.*, 2024, 14, 123.

[11] M. Kostić, S. Najdanović, N. Velinov, M. Radović Vučić, M. Petrović, J. Mitrović, A. Bojić, *Environ. Technol. Innov*., 2022, 26, 102358.

[12] D. Nugroho, K. Wannakan, S. Nanan, R. Benchawattananon, *Sci. Rep.*, 2024, 14, 2455.

[13] M.E. Mahmoud, A.E.H. Abdou, A.K. Shehata, H.M.A. Header, E.A. Hamed, *J. Ind. Eng. Chem.*, 2018, 57, 28.

[14] P. Kannan, S.A. John, *Electrochim. Acta*, 2011, 56, 7029.

[15] M. Lee, P. Amaratunga, J. Kim, D. Lee, *J. Phys. Chem. C*, 2010, 114, 18366.

[16] G. Chang, Y. Luo, W. Lu, X. Qin, A.M. Asiri, A.O. Al-Youbi, X. Sun, *Catal. Sci. Technol.*, 2012, 2, 800.

[17] Shamim Ahmed Khan, Tarun Kumar Misra, *Colloid J*, 2023, 85, 650–65.

[18] O. Cavuslar, E. Nakay, U. Kazakoglu, S.K. Abkenar, C.W. Ow-Yang, H.Y. Acar, *Mater. Adv.*, 2020, 1, 2407.

[19] S.A. Wadhwani, U.U. Shedbalkar, S. Nadhe, R. Singh, B.A. Chopade, Enviro. *Technol. Innov.*, 2018, 9, 186.

[20] S.K. Ghosh, S. Kundu, M. Mandal, T. Pal, *Langmuir*, 2002, 18, 8756.

[21] K.B. Narayanan, H.H. Park, Korean *J. Chem. Eng.*, 2015, 32, 1273.

[22] K. Layek, *Catal. Surv. Asia*, 2023, 27, 349.

[23] F. Svec, Y. Lv, *Anal. Chem.*, 2015, 87, 250–73.

[24] Z. Li, B. Wang, X. Qin, Y. Wang, C. Liu, Q. Shao, N. Wang, J. Zhang, Z. Wang, C. Shen, Z. Guo, *ACS Sustainable Chem. Eng.*, 2018, 6, 13747.

[25] M.R. Malekbala, M.A. Khan, S. Hosseini, L.C. Abdullah, T.S.Y. Choong, *J. Ind. Eng. Chem.*, 2015, 21, 369.

[26] Y. Wang, B. Wang, J. Wang, Y. Ren, C. Xuan, C. Liu, C. Shen, *J. Hazard. Mater.*, 2018, 344, 849.

[27] K. Hormann, T. Müllner, S. Bruns, A. Höltzel, U. Tallarek, *J. Chromatogr. A*, 2012, 1222, 46.

[28] P. Ciambelli, V. Palma, E. Palo, *Catal. Today*, 2010, 155, 92.

[29]L. Kiewidt, J. Thöming, *Chem. Eng. J.*, 2019, 359, 496.

[30] S. Manholi, S. Athiyanathil, *J. Appl. Polym. Sci.*, 2022, 139, 51720.

[31] T. Tanaka, S. Eguchi, H. Saitoh, M. Taniguchi, D.R. Lloyd, *Desalination*, 2008, 234, 175–83.

[32] J. Luo, N. Zhang, R. Liu, X. Liu, *RSC Adv.*, 2014, 4, 64816.

[33] Y. Cao, W. Han, Z. Pu, X. Wang, B. Wang, C. Liu, H. Uyama, C. Shen, *RSC Adv.*, 2020, 10, 26319.

[34] G. Fredi, F. Simon, D. Sychev, I. Melnyk, A. Janke, C. Scheffler, C. Zimmerer, *ACS Omega*, 2020, 5, 19639.

[35] L. Wang, X. Xin, P. Li, J. Dou, X. Han, J. Shen, J. Yuan, *Colloids Surf. B: Biointerfaces*, 2021, 205, 111855.

[36] C.-N. Yu, H.-C. Zhang, S.-X. Su, Y. Liang, *J. Mater. Res. Technol.*, 2021, 15, 6747.

[37] X.-L. Wang, F.-Y. Huang, Y. Zhou, Y.-Z. Wang, *J. Macromol. Sci. B.*, 2009, 48, 710.

[38] Z. Wei, F. Yu, G. Chen, C. Qu, P. Wang, W. Zhang, J. Liang, M. Qi, L. Liu, *J. Appl. Polym. Sci.*, 2009, 114, 1133.

[39] F. Wei, J. Liu, Y.-N. Zhu, X.-S. Wang, C.-Y. Cao, W.-G. Song, *Sci. China Chem.*, 2017, 60,

1236.

[40] A. Baji, S. Wong, T. Liu, T. Li, T.S. Srivatsan, *J. Biomed. Mater. Res.*, 2017, 81B, 343.

[41] S. Du, Y. Luo, Z. Liao, W. Zhang, X. Li, T. Liang, F. Zuo, K. Ding, *J. Colloid Interface Sci.*, 2018, 523, 27–34.

[42] F.-N. Allouche, N. Yassaa, H. Lounici, *Procc Earth Planetc Sci*., 2015, 15, 596.

[43] S. Xie, P. Huang, J.J. Kruzic, X. Zeng, H. Qian, *Sci. Rep.*, 2016, 6, 21947.

[44] C. Galindo, P. Jacques, A. Kalt, *J. Photochem. Photobiol. A: Chem.*, 2000, 130, 35.

[45] F. Sun, J. He, P. Wu, Q. Zeng, C. Liu, W. Jiang, *Chem. Eng. J.*, 2020, 397, 125397.

[46] K. Thangavadivel, G. Owens, P.J. Lesniewski, K. Okitsu, *Ind. Eng. Chem. Res.*, 2013, 52, 18175.

[47] Z. Chen, X. Quan, Y. Xiong, L. Yang, Y. Huang, *Ultrason. Sonochem.*, 2012, 19, 1027–32.

[48] T. Tasaki, T. Wada, K. Fujimoto, S. Kai, K. Ohe, T. Oshima, Y. Baba, M. Kukizaki, *J. Hazard. Mater.*, 2009, 162, 1103.

[49] J. Liu, G. Peng, X. Jing, Z. Yi, *Water Sci. Technol.*, 2018, 78, 936.

[50] Z. Liu, F. Wang, Y. Li, T. Xu, S. Zhu, *J. Environ. Sci.*, 2011, 23, S70.

[51] X. Tao, G. Wang, L. Huang, Q. Ye, D. Xu, *J. Environ. Manage.*, 2016, 184, 480.

Chapter 3

Ultraviolet Encryption Information Storage Using Hydrophobic Poly(ε-caprolactone)/Carbon Quantum Dot Composite Film

3-1. Introduction

With the development of technology, private information leakage often occurs. Therefore, the security of private information has drawn significant attention, information storage is one of topics that are central to the knowledge of the 21st century.[1] Within the realm of materials science, significant attention has been directed towards the development of novel materials for safeguarding information. Considerable research efforts have been devoted to exploring fluorescent materials for applications such as anticounterfeiting materials, [2,3] fluorescent ink, [4,5] and self-erasing materials.[6] However, conventional fluorescent materials are often derived from heavy metals or organic compounds, which suffer from drawbacks like high cost and toxicity, limiting their widespread use. Considering these limitations, the quest for alternative fluorescent materials has become imperative. Quantum dots have emerged as a promising option in recent years due to their unique fluorescent properties and non-toxic nature. Among them, carbon quantum dots (CQDs) have garnered significant attention, owing to advancements in synthesis methods that have significantly reduced production costs.[7,8] Composite materials incorporating CQDs hold immense potential for enhancing information encryption and storage capabilities. Their versatility and compatibility make them promising candidates for addressing the evolving security challenges associated with data storage and protection in the digital age.

Despite significant research efforts focused on hydrogels containing carbon quantum dots (CQDs) for information encryption,[9–11] investigations into composite films remain limited. Film materials offer a distinct advantage over hydrogels due to their higher specific surface area, facilitating more efficient information storage and portability. Compared to metal or inorganic materials, polymers such as polyethylene terephthalate,[12,13] polypropylene,[14,15] and polystyrene[16,17] have been widely used as film materials due to their low cost and high processability.[18] However, excessive use of these films has led to serious environmental problems due to their non-biodegradability.[19] Thus, to foster environmentally sustainable

practices and mitigate plastic pollution, the utilization of biodegradable polymers such as PLA, poly(butylene succinate), poly(vinyl alcohol), and PCL holds significant promise. PCL, a synthetic biodegradable polymer, exhibits the ability to decompose into caprolactone within natural environments, facilitated by the ester groups in its main chain. This degradation process ultimately leads to the metabolization of PCL into CO_2 and H_2O within a relatively short timeframe.[20] Its crystalline temperature, approximately 25°C, enables the formation of an opaque film at room temperature, facilitating easy writing. Additionally, the hydrophobic nature of PCL minimizes water droplet adhesion to the film surface, endowing it with a self-cleaning feature ideal for practical applications.

In this study, a photoluminescent composite film incorporating PCL and nitrogen-doped CQDs (N-CQDs) was prepared for information encryption. The N-CQDs, synthesized through a hydrothermal method, exhibited an excitation-independent photoluminescent property with a high quantum yield (QY) of 17%. The effects of contents of N-CQDs in PCL/N-CQDs films were studied, ranging from 0.1wt% to 0.4wt% relative to PCL. Remarkably, the composite film demonstrated excellent mechanical properties alongside controllable hydrophilicity. Leveraging the fluorescence of N-CQDs, both information encryption and decryption were successfully achieved, which offered a novel approach to information protection and mitigating the risk of information leakage.

3-2. Experimental section

Materials

Citric acid (CA), urea and chloride hexahydrate ($FeCl_3 \cdot 6H_2O$) were commercially purchased from Wako Pure Industries, Ltd. (Osaka, Japan). PCL was purchased from Sigma-Aldrich Co., Ltd (USA). 1,4-dioxane was purchased from Nacalai Tesque, Inc. (Kyoto, Japan). All chemical reagents were used without further purification. Deionized (DI) water purified using a Milli-Q system (Millipore Inc., Milford, MA), was used in all experiments.

Preparation of N-CQDs by hydrothermal method

N-CQDs were prepared using a hydrothermal method based on a previously reported

route.[21,22] Briefly, 1 g of CA and x (x=0.6, 0.8, 1.0) g of urea were dissolved in 10 mL of deionized water. The solution was subjected to ultrasonication for 10 minutes to ensure complete dissolution. The obtained aqueous solution was consequently transferred into a Teflon autoclave reactor (20 mL) and heated at 200 °C for 4 h. Subsequently, the solution was transferred into a 20 mL Teflon autoclave reactor and heated at 200°C for 4 hours. After cooling the autoclave to room temperature, the solution was centrifuged at 11000 rpm for 20 minutes to remove insoluble impurities. Excess moisture was removed via rotary evaporation. The resulting N-CQDs were obtained after freeze-drying for 3 days. The synthesized N-CQDs were denoted as N-CQDs$_{0.6}$, N-CQDs$_{0.8}$, and N-CQDs$_{1.0}$, corresponding to the different amounts of urea used in the synthesis process.

Preparation of PCL/N-CQDs film

The PCL/N-CQDs films were prepared using a solvent casting method. 1,4-dioxane and deionized water were selected as the solvents for PCL and N-CQDs, respectively. Initially, 1.5 g of PCL was dissolved in 19 mL of 1,4-dioxane under magnetic stirring for 4 hours to achieve a homogenous PCL solution. Subsequently, 1 mL of N-CQDs aqueous solution containing N-CQDs at concentrations of 0.1wt%, 0.2wt%, 0.3wt% and 0.4wt% relative to PCL, was added to the PCL solution. Ultrasonication for 40 minutes was employed to enhance the mixing between 1,4-dioxane and deionized water. The resulting homogeneous solution was then transferred to a Petri dish, covered with plastic wrap perforated with holes, and air-dried overnight in an oven at 30°C. Prepared PCL films are named as film 0, film 1, film 2, film 3 and film 4, where represent the contents of N-CQDs as 0wt%, 0.1wt%, 0.2wt%, 0.3wt% and 0.4wt%, respectively.

Characterization

The chemical compositions and functional groups of N-CQDs and N-CQD/PCL films were confirmed by attenuated total reflection Fourier transform infrared spectroscopy (ATR-FTIR, Thermo Scientific Nicolet iS5, USA) at room temperature with a diamond window. All spectra were acquired at 4 cm^{-1} resolutions over 100 scans in the scan range of 500-4000 cm^{-1}.

Elemental compositions of N-CQDs were calculated using X-ray photoelectron spectroscopy (XPS, JEOL JPS-9010MC). The XPS parameters included the power of analysis (wide: 75 W, narrow: 150 W), and monochromatic Al Kα. The survey and high resolution XPS spectra were collected at fixed analyzer pass energies of 160 eV and 10 eV, respectively. To confirm the reproducibility, the measurement was performed over three times for each sample. Binding energies were referred to C-H (Sp3) carbon for C 1s peak set at 284.6 eV. The peaks were fitted by using CasaXPS computer program (Casa Software Ltd). Surface topography of N-CQDs was recorded by AFM at room temperature in air. The size and distribution of N-CQDs were confirmed through Transmission Electron Microscopy (TEM, JEM-2100, JEOL Ltd., Tokyo). Ultraviolet–visible and photoluminescence (PL) spectra of N-CQDs were confirmed using a microplate reader (SH-9000Lab, Yamato Scientific Co., Ltd., Tokyo, Japan). Surface elemental compositions of PCL/N-CQDs films were evaluated by Energy Dispersive Spectrometer (EDS) and X-ray photoelectron spectroscopy (XPS; JPS-9010MC, JEOL, Tokyo, Japan). Water contact angles of PCL/N-CQDs film were measured using a Drop Master DM 300 (Kyowa Interface Science, Saitama, Japan). The water contact angle was measured at 5 s after the contact with 0.5 μL of a water droplet and the value was calculated as the average of 5 different positions for each sample. The tensile behavior of the samples was determined using an AGS-X type tensile tester (Shimadzu, Kyoto, Japan) at room temperature with a maximum speed of 5 mm/min and maximum force of 50 N.

QY calculation of N-CQDs

The QY was calculated by comparing the integrated photoluminescence intensities and absorbance values of the synthesized N-CQDs with the ones of the quinine sulfate.[23]

$$QY=(QY_0\times Grad\times\eta_0^2)/(Grad_0\times\eta^2) \quad (3\text{-}1)$$

In the equation Grad represents the gradient derived from the plot of integrated fluorescence intensity versus absorbance. η denotes the refractive index. The subscript 0 refers to the reference fluorophore, quinine sulfate, possessing a known QY of 0.54. The η value for quinine sulfate in 0.1 M H_2SO_4 and for the water solutions of nanocomposites was 1.33.

Information loading

Surface loading of information onto PCL/N-CQDs was achieved via ionoprinting method.[24] Briefly, filter paper was immersed in a $FeCl_3$ solution (125 mM) for 2 hours, and then it was cut into the desired shapes and placed onto the surface of the PCL/N-CQDs film for 5 min. The filter paper was subsequently removed, and the desired information loading was obtained, which was only visualized under specific UV light.

3-3. Result and discussion

Chemical components

The chemical compositions of N-CQDs were confirmed through FT-IR measurement, and the spectra are presented in **Figure 3-1(a)**. Stretching vibration absorption peaks of C=O or C=N, C-N and C-O were observed at 1660 cm^{-1}, 1185 cm^{-1} and 1047 cm^{-1}. The absorption bands in the range of 1412-1346 cm^{-1} corresponded to the stretching vibration of C-N from aromatic amine groups. The carboxylate COO^- asymmetric stretching band was observed at 1550 cm^{-1}. A broad peak around 3000 cm^{-1} indicated the stretching vibration of N-H and O-H, confirming the good solubility of N-CQDs in water.[25] Comparative analysis revealed that in the spectra of N-CQDs$_{1.0}$ and N-CQDs$_{0.8}$, the content of C-N groups increased, and the peak corresponding to C=N components became more pronounced compared to the N-CQDs$_{0.6}$. These results suggest that increasing the dopant content appropriately enhances the doping effect.

Surface chemical compositions and structures of N-CQDs were analyzed by XPS measurement. The survey spectra and elemental contents are depicted in **Figure 3-1(b)** and **Figure 3-2**. The analysis revealed that N-CQDs consist predominantly of carbon, nitrogen, and oxygen elements, as evidenced by the peaks corresponding to C 1s, N 1s, and O 1s with binding energies of 285.8 eV, 399.5 eV, and 531.4 eV, respectively. Notably, the presence of nitrogen with concentrations exceeding 10% was observed in all samples, indicating successful nitrogen doping modification. Furthermore, the lowest C/O and C/N ratios were observed in the sample synthesized with CA/urea ratio of 5:4, suggesting that N-CQDs$_{0.8}$ possessed more functional groups.

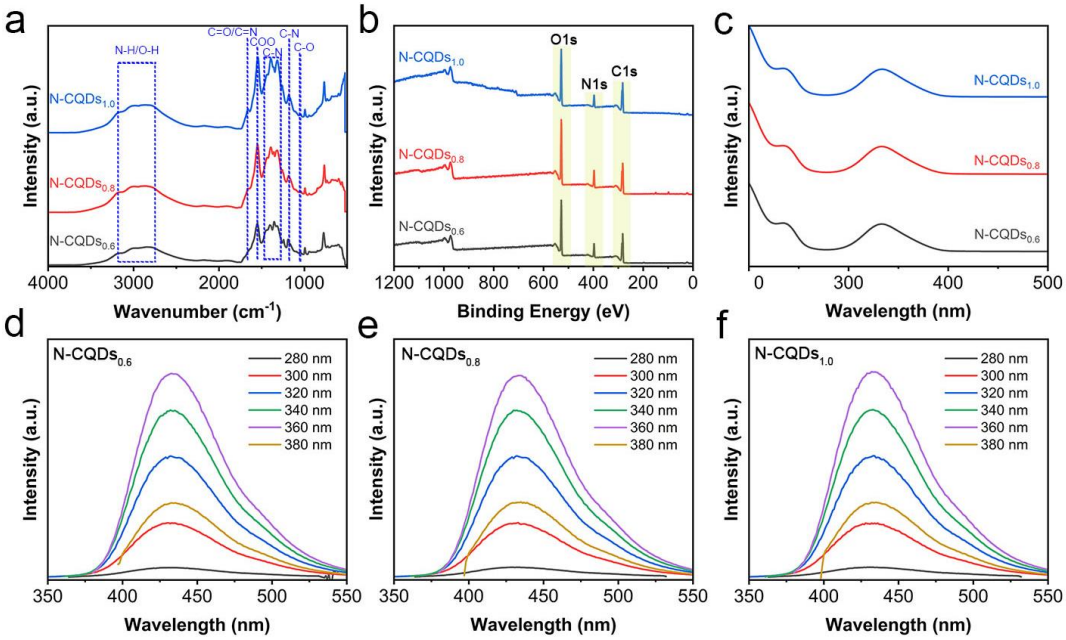

Figure 3-1. (a) FTIR spectra, (b) XPS survey, (c) UV-vis spectra, and (d-f) Florescent spectra of N-CQDs.

Further insights into the chemical composition of N-CQDs were obtained through detailed analysis of the C 1s, O 1s, and N 1s fine spectra derived from XPS results, as illustrated in **Figure 3-2**. The C 1s spectrum exhibited three distinct peaks at binding energies of 284.6 eV, 286.0 eV, and 288.0 eV, corresponding to C-C/C=C, C-N, and O=C-O bonds, respectively. Similarly, the N 1s spectrum revealed three discernible peaks at binding energies of 399.5 eV, 400.5 eV, and 401.4 eV, attributed to pyridinic N, pyrrolic N, and graphitic N, respectively. [26] Regarding the O1s spectrum, two peaks were observed at binding energies of 531.4 eV and 532.8 eV, corresponding to C=O and C-O bonds, respectively. The combined results from FTIR and XPS analyses suggest that nitrogen from urea was successfully incorporated into the N-CQDs in the form of C-N and C=N bonds, contributing to their functionalization

Optical and fluorescent properties of N-CQDs

The optical properties of N-CQDs were investigated using a UV-vis spectrometer, and the spectra are presented in **Figure 3-1(c)**. Two distinct absorbance peaks were observed at wavelengths of 344 nm and 234 nm, respectively. Interestingly, there was no discernible difference in the UV-vis spectra among N-CQDs synthesized with different dopant contents.

This suggests that variations in dopant content within a certain range have minimal impact on the optical properties of N-CQDs. The peak at 243 nm can be attributed to the π-π* electronic transitions of C=C and C=N bonds of the sp^2 carbon domain.[27,28] This transition typically results in negligible photoluminescence.[29] Conversely, the peak observed at 344 nm is assigned to the n-π* transition of C=O or C=N bonds presented in the structure of N-CQDs.[29–31]

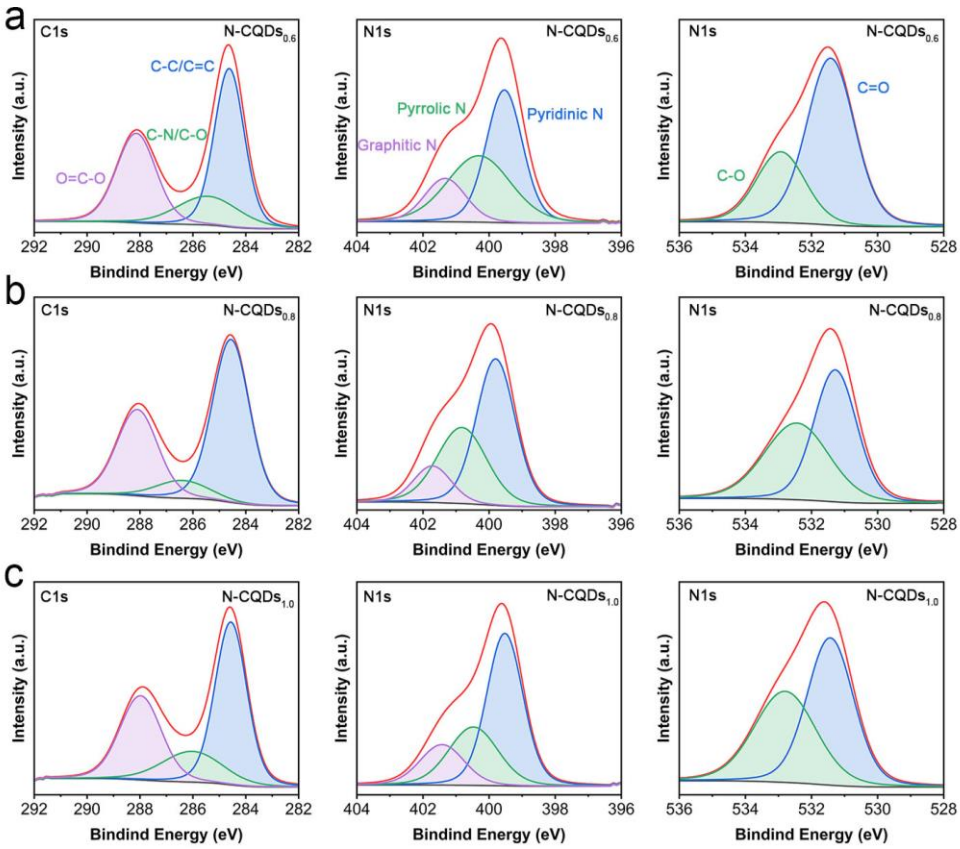

Figure 3-2. High-resolution XPS C 1s, N 1s and O 1s spectra of (a) N-CQDs$_{0.6}$, (b) N-CQDs$_{0.8}$, and (c) N-CQDs$_{1.0}$.

The fluorescent spectra depicted in **Figure 3-1(d-f)** exhibited fluorescent emission wavelengths (λ_{em}) at 432 nm across a range of excitation wavelengths (λ_{ex}) from 280 nm to 380 nm, demonstrating an excitation-independent photoluminescent property. Notably, the maximum intensity of the emission peak was observed at λ_{ex} of 360 nm with the full width at half maximum of 68 nm. The QY values were calculated using quinine sulfate as a reference, and the results are shown in **Table 3-1**. Remarkably, the highest QY was obtained for N-CQDs$_{0.8}$, suggesting that a higher dopant content does not necessarily correlate with a better fluorescence yield. This observation aligns with the XPS analysis, which revealed elevated levels of C=N

and C=O groups in N-CQDs$_{0.8}$. It is postulated that these functional groups act as electron donors or acceptors, facilitating charge transfer processes that enhance the fluorescence QY.

Compared the QY values of N-CQDs synthesized from CA/urea in this work with those reported in literature,[21,23] it's evident that the N-CQDs$_{0.8}$ exhibited relatively high QY value. Typically, urea-doped CQDs synthesized from citric acid using microwave methods have QY values ranging from 8% to 15%.[23] Compared to microwave method, the hydrothermal method employed in our research appears to be more effective in achieving N-CQDs with superior QY. Notably, N-CQDs$_{0.8}$, with its optimized composition, was selected for further investigation in subsequent discussions.

Table 3-1. λ_{ex}, $\lambda_{em,}$ and QY value of N-CQDs synthesized from CA/urea with different methods in this work and previous literature reports

Methods	λ_{ex}	λ_{em}	QY(%)	Reference
Hydrothermal	360	432	17.45	CQDs$_{0.6}$ in this work
Hydrothermal	360	432	17.55	CQDs$_{0.8}$ in this work
Hydrothermal	360	432	17.48	CQDs$_{1.0}$ in this work
Microwave	400	522	7.50	[23]
Microwave	420	540	14.00	[32]
Microwave	410	450	15.00	[33]

Morphologies of N-CQDs

The morphologies of N-CQDs were investigated by TEM and the images, as shown in **Figure 3-3**. The images reveal the spherical nature of N-CQDs nanoparticles with good dispersion. Size distribution analysis, conducted using TEM images from over 50 data points, is illustrated in **Figure 3-3(b),** indicating an average particle size of 21.5 nm. This size is well-suited to the morphological characteristics expected of quantum dots. Previous studies have suggested that the size of N-CQDs derived from CA/urea mixtures can vary from 2 nm to 16 nm.[34] It is likely that some degree of aggregation occurred during the sample preparation process for TEM observation.

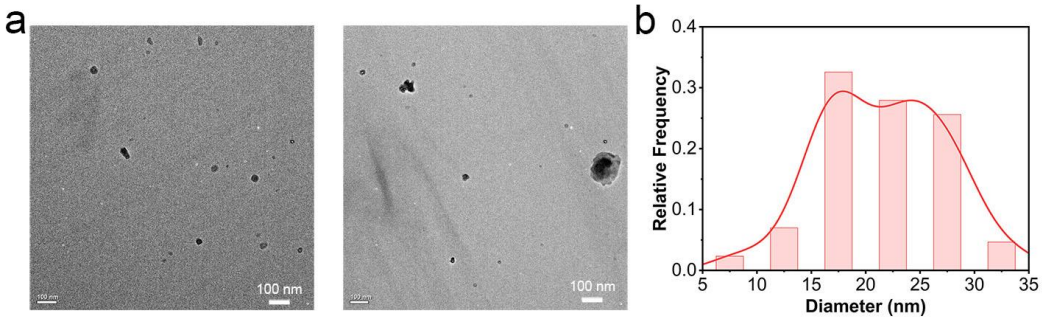

Figure 3-3. (a) TEM images of N-CQDs$_{0.8}$ from different regions. (b) size distribution of N-CQDs$_{0.8}$.

Characterization of PCL/N-CQDs film

The elemental composition of pristine PCL film and PCL/N-CQDs films was investigated using EDS measurements, with results presented in **Table 3-2**. Upon composite formation with N-CQDs, surface analysis revealed the presence of three elements: C, N, and O. Notably, nitrogen exhibited an atomic ratio of approximately 15%, with the highest concentration observed in film$_2$.

Table 3-2. Elemental atomic ratios on the surface of PCL/N-CQDs films derived from EDS measurements

Sample	C	O	N
Film$_0$	74.096	25.904	
Film$_1$	60.861	23.872	15.267
Film$_2$	58.865	23.860	17.276
Film$_3$	65.672	20.181	14.147
Film$_4$	59.841	23.800	16.360

The hydrophilicity of PCL/N-CQDs films was investigated using water contact angle measurement, with the results presented in **Figure 3-4(a)**. The neat PCL film showed a water contact of 100.2° owing to its inherently hydrophobic nature. An increase in water contact angle was observed as the content of N-CQDs in the PCL/N-CQDs film increased. It is worth noting that the PCL/N-CQDs film transitioned to a hydrophilic state when the N-CQDs content

surpassed 0.3%. Within the composite film, the evenly distributed N-CQDs functioned as fillers. Compared to film 0, some of N-CQDs in film 1 were exposed to the surface, increasing the roughness, lowering the surface energy, and leading to an increase in water contact angle.[35] As the N-CQDs content increased, the inherently hydrophilic nature of N-CQDs contributed to a corresponding increase in the water contact angle value of the composite film.

The mechanical properties of PCL/N-CQDs films were conducted by tensile tests with the results presented in **Figure 3-4(b)** and **Table 3-3**. The elastomeric properties of PCL were evident in PCL/N-CQDs films, characterized by high elongation at break. The composite film Compared with neat PCL film, the deformation behavior during the stretching process didn't change after N-CDQs were added. What's more, the tensile strength was improved from 32.39 MPa of film 0 to 45.44 MPa of film 2, and the elongation at break was improved from 947.35% of $film_0$ to 1342.56% of film 2, indicating that the N-CQDs can be used as reinforcing agents to enhance the mechanical properties of the film. Based on these results, the film 2 was selected for next study.

Table 3-3. Mechanical properties of PCL/N-CQDs films

Sample	Tensile strength (MPa)	Elongation at break (%)
$Film_0$	32.39±4.70	947.35±89.47
$Film_1$	30.36±0.34	1025.47±67.98
$Film_2$	45.44±0.56	1342.56±67.51
$Film_3$	45.23±2.51	1326.21±41.37
$Film_4$	41.34±6.92	1095.87±139.18

Information encryption

It has been reported that the fluorescence of N-CQDs can be quenched by Fe^{3+}, demonstrating the potential of the composite film for information encryption. As depicted in **Figure 3-4(c)**, upon ionoprinting with Fe^{3+}, a predefined pattern of the alphabet "U" became readily visible on the surface of the PCL/N-CQDs film under UV irradiation, while remaining undetectable under visible light. The fluorescent characteristics of N-CQDs serve to fulfill the

function of information protection and encryption. Additionally, the opacity of the composite film enables the pattern to be easily discerned without requiring a background panel.

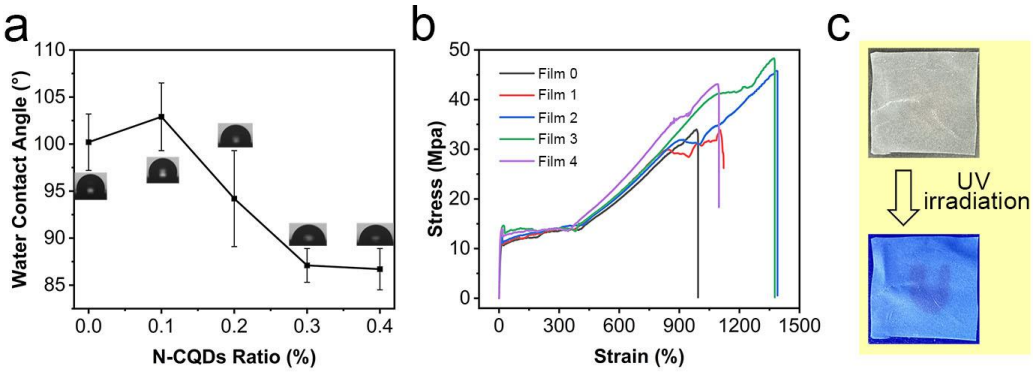

Figure 3-4. (a) Water contact angle and (b) tensile stress-strain curves of neat PCL film and PCL/N-CQD films. (c) Photos of the ionoprinting process of PCL/N-CQDs film under visible and UV light.

3-4. Conclusions

Photoluminescent N-CQDs were successfully synthesized from CA and urea using the hydrothermal method. The impact of the dopant quantities was investigated with three different CA/urea ratios. Doping modifications were assessed through FT-IR and XPS measurements, revealing enhanced doping outcomes with optimal dopant levels. A CA/urea ratio of 5:4 yielded higher N contents and C-N functional group contents. The synthesized N-CQDs exhibited favorable optical properties, with a distinct absorbance peak at 344 nm and excitation-independent photoluminescent characteristics. The maximum intensity of λ_{em} was obtained at λ_{ex} of 360 nm. With an average diameter of 21.5 nm, the N-CQDs demonstrated nanoscale dimensions consistent with quantum dot morphology.

PCL/N-CQDs composite films were fabricated with varying N-CQDs contents ranging from 0.1wt% to 0.4wt%. Even distribution of N-CQDs on the film surface was confirmed via EDS analysis. The hydrophilicity of PCL/N-CQDs films was adjustable within a considerable range, from 100.2° to 86.7°, by varying the N-CQDs content. Preservation of PCL's hydrophobic nature was observed at lower N-CQDs contents, offering practical benefits for applications. Furthermore, the resultant PCL/N-CQDs film retained the photoluminescent properties of N-CQDs, enabling information encryption via ionoprinting technique. This opaque, hydrophobic, and photoluminescent composite film holds significant potential for applications in information encryption.

3-5. References

[1] H. Wang, X. Ji, Z. A. Page, J. L. Sessler, *Mater. Chem. Front.*, **2020**, *4*, 1024.

[2] W. Ren, G. Lin, C. Clarke, J. Zhou, D. Jin, *Adv. Mater.*, **2020**, *32*, 1901430.

[3] Y. Song, M. Lu, G. A. Mandl, Y. Xie, G. Sun, J. Chen, X. Liu, J. A. Capobianco, L. Sun, *Angew. Chem. Int. Ed.*, **2021**, *60*, 23790.

[4] J. Du, L. Sheng, Y. Xu, Q. Chen, C. Gu, M. Li, S. X. Zhang, *Adv. Mater.*, **2021**, *33*, 2008055.

[5] E. R. Sauvé, C. M. Tonge, Z. M. Hudson, *J. Am. Chem. Soc.*, **2019**, *141*, 16422.

[6] Z. Chen, Y. Chen, Y. Guo, Z. Yang, H. Li, H. Liu, *Adv. Funct. Mater.*, **2022**, *32*, 2201009.

[7] Y. Wang, A. Hu, *J. Mater. Chem. C*, **2014**, *2*, 6921.

[8] S. Zhu, Q. Meng, L. Wang, J. Zhang, Y. Song, H. Jin, K. Zhang, H. Sun, H. Wang, B. Yang, *Angew. Chem. Int. Ed.*, **2013**, *52*, 3953.

[9] Q. Wang, Z. Qi, Q. Wang, M. Chen, B. Lin, D. Qu, *Adv Funct. Mater.*, **2022**, *32*, 2208865.

[10] J. Chen, G. Chen, C. Wu, B. Lei, Y. Liu, M. Zheng, *J. Mater. Chem. C*, **2023**, *11*, 16177.

[11] Q. Luo, H. Liu, D. Li, J. Dai, L. Xia, J. Jiang, Y. Xu, B. Zeng, W. Luo, L. Dai, *Carbohydr. Polym.*, **2024**, *326*, 121610.

[12] R. Nisticò, *Polym. Test.*, **2020**, *90*, 106707.

[13] Y. Wang, X. Wang, W. Lu, Q. Yuan, Y. Zheng, B. Yao, *Talanta.*, **2019**, *198*, 86.

[14] Z. Honarvar, M. Farhoodi, M. R. Khani, A. Mohammadi, B. Shokri, R. Ferdowsi, S. Shojaee-Aliabadi, *Carbohydr. Polym.*, **2017**, *176*, 1.

[15] S.-Y. Sung, L. T. Sin, T.-T. Tee, S.-T. Bee, A. R. Rahmat, W. A. W. A. Rahman, A.-C. Tan, M. Vikhraman, *Trends Food Sci. Technol.*, **2013**, *33*, 110.

[16] E. Syranidou, K. Karkanorachaki, F. Amorotti, M. Franchini, E. Repouskou, M. Kaliva, M. Vamvakaki, B. Kolvenbach, F. Fava, P. F.-X. Corvini, N. Kalogerakis, *Sci. Rep.*, **2017**, *7*, 17991.

[17] E. Ferrari, P. Fabbri, F. Pilati, *Langmuir*, **2011**, *27*, 1874.

[18] V. Siracusa, P. Rocculi, S. Romani, M. D. Rosa, *Trends Food Sci. Technol.*, **2008**, *19*, 634.

[19] J. S. Lyu, J.-S. Lee, J. Han, *Sci. Rep.*, **2019**, *9*, 20236.

[20] C. Zhu, T. Li, M. M. Mohideen, P. Hu, R. Gupta, S. Ramakrishna, Y. Liu, *Polymers*, **2021**, *13*, 744.

[21] B. Vercelli, R. Donnini, F. Ghezzi, A. Sansonetti, U. Giovanella, B. La Ferla, *Electrochim.*

Acta., **2021**, *387*, 138557.

[22] X. Lai, C. Liu, H. He, J. Li, L. Wang, Q. Long, P. Zhang, Y. Huang, *Ferroelectrics*, **2020**, *566*, 116.

[23] E. F. C. Simões, J. M. M. Leitão, J. C. G. E. Da Silva, *Microchim. Acta.*, **2016**, *183*, 1769.

[24] X.-X. Le, W. Lu, J. He, M. J. Serpe, J.-W. Zhang, T. Chen, *Sci. China Mater.*, **2019**, *62*, 831.

[25] F. Wang, P. Chen, Y. Feng, Z. Xie, Y. Liu, Y. Su, Q. Zhang, Y. Wang, K. Yao, W. Lv, G. Liu, *Appl. Catal. B: Environ.*, **2017**, *207*, 103.

[26] P. Zhao, B. Jin, Q. Zhang, R. Peng, *Langmuir*, **2021**, *37*, 1760.

[27] L. Chen, Y. Peng, J.-E. Lu, N. Wang, P. Hu, B. Lu, S. Chen, *Int. J.Hydrogen Energy*, **2017**, *42*, 29192.

[28] J. Shang, L. Ma, J. Li, W. Ai, T. Yu, G. G. Gurzadyan, *Sci. Rep.*, **2012**, *2*, 792.

[29] Z. L. Wu, M. X. Gao, T. T. Wang, X. Y. Wan, L. L. Zheng, C. Z. Huang, *Nanoscale*, **2014**, *6*, 3868.

[30] H.-J. Li, X. Sun, F. Xue, N. Ou, B.-W. Sun, D.-J. Qian, M. Chen, D. Wang, J. Yang, X. Wang, *ACS Sustainable Chem. Eng.*, **2018**, *6*, 1708.

[31] M. Chen, W. Wang, X. Wu, *J. Mater. Chem. B*, **2014**, *2*, 3937.

[32] S. Qu, X. Wang, Q. Lu, X. Liu, L. Wang, *Angew. Chem.*, **2012**, *124*, 12381.

[33] W. Kasprzyk, T. Świergosz, S. Bednarz, K. Walas, N. V. Bashmakova, D. Bogdał, *Nanoscale*, **2018**, *10*, 13889.

[34] J. D. Stachowska, A. Murphy, C. Mellor, D. Fernandes, E. N. Gibbons, M. J. Krysmann, A. Kelarakis, E. Burgaz, J. Moore, S. G. Yeates, *Sci. Rep.*, **2021**, *11*, 10554.

[35] S. A. Vyavahare, A. P. More, *Polym. Bull.*, **2024**.

Concluding remarks

In this doctoral dissertation, functionalization of PCL was achieved through surface modification and filler modification methods. To preserve the inherent biodegradability of PCL, the chemical structure was not changed. Various applications were developed with these functionalized materials based on PCL.

In chapter 1, the functionalization of PCL film was successfully achieved via surface oxidation method using light-activated $ClO_2^{\bullet}$ gas. After oxidation, some oxygen-containing functional groups were introduced onto the surface of the PCL film, improving the hydrophilicity of PCL with an increase of water contact angle from 99.1°±1.1° to 66.2°±5.7°. The oxidation mechanism was investagited through ^{1}H-NMR and GPC measurements, which indicated the scission of PCL molecules on the surface of the film into smaller segments via radical gases from the ester groups. Additionally, electroless copper plating demonstrated successful copper deposition on oxidized PCL film, which showed an potential to be used as a conductive material.

In chapter 2, the functionlization of PCL monolith was achieved through surface modification method using PDA. After coated with PDA, the PDA-PCL monolith exhibited improved hydrophilicity permitting its further application in aqueous solution. The PDA-PCL monolith was utilized as a catalyst carrier for Au particles. An effective catalytic reactor was successfully fabricated as the format of Au@PDA-PCL monolith. This reactor showed the highest catalytic efficiency of 98.54% for MO and showed a good reusability.

In chapter 3, the functionalized of PCL film was achieved via filler modification with CQDs. A photoluminescent composite film was prepared incorporating CQDs and PCL. The photoluminescent of CQDs was enhanced using a dope modification method, and the impact of the dopant quantities was investigated with three different CA/urea ratios. The hydrophilicity of PCL/N-CQDs films was adjustable within a considerable range, from 100.2° to 86.7°, by varying the N-CQDs content. Furthermore, the resultant PCL/N-CQDs film retained the photoluminescent properties of N-CQDs, enabling information encryption via ionoprinting technique. This opaque, hydrophobic, and photoluminescent composite film holds significant potential for applications in information encryption.

List of Publications

1. Surface Oxidation of Poly(ε-caprolactone) Using Chlorine Dioxide Radical Gas

Yu Cao, Yu-I Hsu*, Hiroshi Uyama*

Reactive and Functional Polymers, **2024**, *200*, 105912.

DOI: /10.1016/j.reactfunctpolym.2024.105912

2. Development of a Flow Reactor Incorporating Polydopamine-Poly(ε-caprolactone) with Gold Particles

Yu Cao, Yu-I Hsu*, Hiroshi Uyama*

Journal of Industrial and Engineering Chemistry

Under review

3. UV Encryption Information Storage Using Hydrophobic Poly(ε-caprolactone)/Carbon Quantum Dot Film

Yu Cao, Yu-I Hsu*, Hiroshi Uyama*

Materials letters

Under view

Acknowledgements

This study was carried out from 2021 to 2024 at the Department of Applied Chemistry, Graduate School of Engineering, Osaka University. The doctoral dissertation focused on functionalization and applications of polymer materials based on PCL. This work would not have been possible without the support and assistance of those around me, and I am deeply grateful to all of them for their kindness over the three years.

First and foremost, I am thankful to Osaka University for providing me with the opportunity to pursue my research. I am also grateful to the QLEAR Fellowship for providing me with financial support for one and a half years, which enabled me to focus on my studies without financial concerns.

I extend my heartfelt appreciation to my supervisor, Prof. Hiroshi Uyama. for his invaluable guidance and unwavering support throughout my PhD journey. His advice and encouragement have been instrumental in my research progress. I would also like to thank the other members of my thesis committee, Prof. Takahiro Kozawa and Prof. Satoshi Minakata, for their insightful comments and valuable advice.

Additionally, I appreciate Prof. Yu-I Hsu, Associate Professor in our group. She gave me me a lot of inspiration and suggestion at the biggening of my research. Besides, I received many kind helps from her in my experiments and paper writing. And I also appreciate Assistant Prof. Akihide Sugawara for his advices to my experiment. He gave my many wonderful memories. I am deeply thankful to Prof. Susumu Kuwabata and Assoc. Prof. Taro Uematsu for their assistance with TEM measurements for my study.

My gratitude also extends to everyone who has worked at Uyama Laboratory, both former and current: Ms. Yoko Uenishi, Ms. Tomoko Shimizu, Ms. Erina Katsuragawa, Ms. Chikako Abe, Ms. Rieko Yagi, Ms. Yasushi Takeuchi, Ms. Yasuko Matsuda, Ms. Kyoko Fukuma.

I would like to express my utmost gratitude to all members in Uyama Laboratory between 2021 and 2024 for hearty supports and kind assistances in research and daily life. Exclusively, I would like to thank to: Dr. Meng Wei, Dr. Yan Wang, Dr. Luwei Zhang, Dr. Mark Adam Malaluan Ferry, Dr. Yuxiang Jia, Dr. Nontarin Roopsung, Dr. Manjie He, Dr. Emil Hajili, Dr.

Madhurangika Panchabashini Horathal Pedige, Dr. Peng Du, Dr. Juan Wang, Dr. Kazuki Shibasaki, Dr. Atsuki Takagi, Dr. May Myat Noe, Dr. Guan Wang, Dr. Ying Yao, Dr. Hasinah Binti Mohamed Rafiq, Dr. Judit Rebeka Molnar. Dr. Ruiqi Zhang, Dr. Yihan Gao, Dr. Izzah Binti Haji Abdul Hamid Durrati, Dr. Sooyeon Noh, Dr. Jiahui Dong, Dr. Yazhou Su, Dr. Kai Cheng, Dr. Qianying Li, Dr. Yihe Chen, Ms. An Thuy Le Huynh, Mr. Xinyu Lou, Ms. Rika Onishi, Mr. Hiroshi Hasegawa, Mr. Shotaro Yano, Mr. Kippei Yamamura, Mr. Alejandro Adrian Ayala Escamilla, Mr. Ziyu Meng, Ms. Shafri Shafinee Yarnina Hj Md, Ms. Akane Odagaki, Ms. Rina Kugimiya, Mr. Shunya Kubo, Mr. Sota Nakagawa, Ms. Maoko Hayashi, Ms. Daniela Yacine Sebastião Bravo Da Costa. Mr. Kohnosuke Yoshida, Ms. Chua Siaw Thong, Ms. Peixuan Shao, Mr. Yuchen Zhang, Mr. Naoaki Ishihara, Mr. Yuta Okuda, Ms. Kanako Sakai, Mr. Yuta Kitagaki, Mr. Daiki Morimoto, Mr. Yudai Ioku, Mr. Takehiro Masuda, Ms. Akari Ito, Mr. Yuto Kirihata, Mr. Yuto Shibamoto, Mr. Taiga Hamabe, and Ms. Chiho Yamaji.

Finally, I would like to extend my heartfelt appreciation to my family members for their thoughtful attention and unwavering encouragement.

June 2024

Yu Cao